Molecular dynamics studies of electron-ion temperature equilibration in hydrogen plasmas within the coupled-mode regime

Lorin X. Benedict, Michael P. Surh, Liam G. Stanton, Christian R. Scullard, Alfredo A. Correa, John I. Castor, and Frank R. Graziani
Lawrence Livermore National Laboratory, Livermore, California 94550, USA

Lee A. Collins, Ondřej Čertík, and Joel D. Kress
Los Alamos National Laboratory, Los Alamos, New Mexico 87545, USA

Michael S. Murillo
Department of Computational Mathematics, Science and Engineering, Michigan State University, East Lansing, Michigan 48824, USA
(Received 7 December 2016; published 10 April 2017)

We use classical molecular dynamics (MD) to study electron-ion temperature equilibration in two-component plasmas in regimes for which the presence of coupled collective modes has been predicted to substantively reduce the equilibration rate. Guided by previous kinetic theory work, we examine hydrogen plasmas at a density of $n = 10^{26}$ cm^{-3}, $T_i = 10^5$ K, and 10^7 K $< T_e < 10^9$ K. The nonequilibrium classical MD simulations are performed with interparticle interactions modeled by quantum statistical potentials (QSPs). Our MD results indicate (i) a large effect from time-varying potential energy, which we quantify by appealing to an adiabatic two-temperature equation of state, and (ii) a notable deviation in the energy equilibration rate when compared to calculations from classical Lenard-Balescu theory including the QSPs. In particular, it is shown that the energy equilibration rates from MD are more similar to those of the theory when coupled modes are neglected. We suggest possible reasons for this surprising result and propose directions of further research along these lines.

DOI: 10.1103/PhysRevE.95.043202

I. INTRODUCTION

The phenomenon of electron-ion temperature equilibration is important for the study of inertial confinement fusion (ICF), since the asymmetric manner in which α-particle fusion products deposit energy naturally creates such a temperature (T) split at certain key regions and times within an imploding capsule [1,2]. While much of the ICF capsule material is a 50-50 mixture of deuterium and tritium, the presence of an outer so-called ablator layer in such capsules creates the possibility of admixture of higher-Z (ionic charge) elements (C, Be, and/or dopants like Ge and W) into the deuterium-tritium (DT) fuel. This in turn introduces significant complexities for the theoretical description of the T-equilibration process, because such ions serve to make the plasma more strongly coupled. Since modeling of electron-ion T equilibration is a necessary part of integrated simulations of ICF, the problems of T equilibration in both low-Z and high-Z–low-Z mixtures are therefore of concern [3].

Recent work on T equilibration has involved both kinetic theory of various types [4–8] and MD simulations with like charges and the pure Coulomb interaction [8,9] as well as opposite-charge simulations with quantum statistical potentials (QSPs) to mock up the effects of quantum diffraction [10–14]. All but a few of these studies [7,11,14] confined themselves to pure hydrogen (or the proton-positron system [8,9]). Even for H, the demonstration of agreement between molecular dynamics (MD) results and kinetic theory took some time [10–13], in part because the effect of using the QSPs changes the result slightly even in weak coupling [11]. For the classical like-charge proton-positron system, demonstration of agreement was somewhat more straightforward, motivating a clear connection between the classic Landau-Spitzer equilibration rate [15] derived from the Fokker-Planck equation and a generalized Lenard-Balescu [16] scheme in which both dynamical screening and two-body static correlations (in the form of local-field corrections) are included [8]. Furthermore, it was shown that for many regimes of interest to ICF, the complex dynamical screening of the two-component (electron-proton) plasma could be replaced by the static response of the electrons alone, yielding identical results [8,9,12,13]. This is hardly surprising, since in a given electron-proton collision, the spectator electrons are expected to move much faster than the much heavier spectator protons. It is in this sense that a description of the collision rate in terms of a Coulomb logarithm $\ln \lambda_{ei} = \ln(b_{\max}/b_{\min})$ is sensible, where the maximum impact parameter $b_{\max}$ is identified with the static electron-only Debye length. Such simplifications in turn form the basis for analytic in-line models of electron-ion T equilibration widely used in ICF simulation codes [1,2].

However, as was pointed out early on by Dharma-wardana and Perrot [4,17], this failure of the ions to participate in the screening may not hold in general. Indeed, coupled modes of the electron-ion system are known to exist in the form of ion acoustic waves (analogous to phonons in a solid) and their presence is expected to alter the equilibration rate relative to that predicted by a theory in which independent electron and ion plasma waves are solely responsible for the exchange of energy in a two-temperature (2T) plasma. A regime in which coupled modes were argued to be important is that accessed in the intense laser irradiation of condensed matter [18]: solid density and $T_e \gg T_i$. Roughly a decade after this work, Gericke and co-workers [19–21] used the Lenard-Balescu kinetic equation to study both the nature of the effect of coupled modes on T equilibration and the precise regime where they are expected to be important for

 ©2017 American Physical Society

weakly coupled systems. By analyzing the detailed structure of the two-component dynamical dielectric function, the authors of Ref. [20] presented this condition for the importance of coupled modes for a plasma with electrons and a single species of ions [22]:

$$T_i \lesssim 0.27(Z_i T_e) \tag{1}$$

for nondegenerate electrons; here Z_i is the charge of the ion. For hydrogen ($Z_i = 1$), T_e must be at least 4 times larger than T_i for coupled modes to have an effect. This is not the typical scenario in ICF, at least within the region of undoped DT fuel. However, if Z_i is greater than 4, the above condition suggests that theoretical treatments that neglect coupled modes, such as the Landau-Spitzer theory, may be suspect even for $T_e \sim T_i$.

In the work of Ref. [20], comparisons were made between the so-called coupled-mode theory (perturbative treatment of the Lenard-Balescu theory including dynamical screening) and the Fermi golden rule (FGR) theory [4] (analogous treatment, but where the ion f-sum rule is used to reduce the screening to that of the static response of the electrons [8,20]). The systems considered were hydrogen at a particle density $n = 10^{26}$ cm^{-3} and species temperatures $T_i = 10^5$ K and 10^5 K $< T_e < 10^{10}$ K. It was predicted that the presence of coupled modes reduces the energy equilibration rate by up to ∼50% relative to that predicted by the FGR theory and other approaches akin to the Landau-Spitzer theory. The fact that it is a reduction is easy to understand: Ion-acoustic waves are modes in which a significant fraction of the electrons form screening clouds that move with the ions. Such concerted motion is not conducive to resistive heating of ions by electrons (or vice versa), for precisely the same reason that energy transfer is not permitted in a simulation in which the Born-Oppenheimer approximation is invoked (electrons slaved to the ion dynamics). The work of Ref. [20] is the first we know of to attempt to fully quantify this effect for hydrogen plasmas.

As we have already implied, the presence of coupled modes renders the theoretical description sufficiently complex so that a simple analytic representation of the T-equilibration rate is no longer possible. The potential importance for ICF simulations, however, has prompted researchers to search for approximate expressions that capture the salient features of the reduction in the rate due to ion-acoustic waves [19,23]. The work of Chapman *et al.* in Ref. [23] is particularly notable for its accuracy in this regard, but its application in ICF simulations [24] incurs significant computational expense relative to the simpler theories that neglect coupled modes such as the Landau-Spitzer theory and its many variants [12,13,15].

Because the aforementioned predictions of the coupled-mode (CM) effect in T equilibration used a variant of kinetic theory that is expected to be exact only in the limit of weak coupling [16], it is reasonable to ask if these predictions are accurate in practical realizations of out-of-equilibrium hydrogen plasmas. To this end, Vorberger and Gericke searched through the existing MD results [8,9,11–14,25] to assess if simulations within the regime of interest for coupled modes had been performed [26]. Their conclusion was that only one simulation *might* have exhibited the CM effect [25]. This observation, together with the fact that experimental measurements of T equilibration in plasmas are practically nonexistent, emphasizes the need for dedicated MD simulations specifically tailored to measure the effect of coupled modes on the relaxation rates. This would in turn aid in the development of more accurate in-line models for use in ICF codes, by buttressing our confidence in the theories used to construct such models [19,23], and/or critiquing their assumptions if their predictions are shown to be inaccurate.

In this work we study temperature equilibration with nonequilibrium classical MD simulations for plasmas that are chosen to lie squarely within the regime indicated by Eq. (1): hydrogen at a density of $n = 10^{26}$ cm^{-3} and $T_e \gg T_i$. These are chosen to coincide with the plasmas studied in Ref. [20]. We model the interparticle interactions in these plasmas by Dunn-Broyles diffractive [27] and Minoo *et al.* exchange [28] QSPs [29]. For each plasma studied, we compare our MD results to both the coupled-mode Lenard-Balescu (LB) theory of T equilibration and the FGR (neglecting coupled modes) theory. Since we invoke an approximate description of these hydrogen plasmas in which the electrons are classical particles that interact via effective T-dependent interactions, we take care to apply the CM LB and FGR theories to the classical QSP system rather than to the quantum Coulomb system as done in Ref. [20], to ensure that effects arising from the assumption of classical electrons and altered effective interactions are included appropriately [11].

We present and discuss several prominent MD results here, for these specific hydrogen cases:

(i) The temperature relaxation is asymmetric, $dT_e/dt \neq -dT_i/dt$, indicating sizable contributions to dT_e/dt and dT_i/dt from time-varying potential energy V. This effect is beyond the weak-coupling treatment of standard Lenard-Balescu theory (which only conserves kinetic energy), but it has been discussed and studied before in numerous theoretical contributions [3,7,21] and has been noted in at least one previous classical MD study [14]. We define and extract an effective two-temperature thermodynamic potential $E(T_i, T_e)$ (with associated heat capacities $C_e = \partial E/\partial T_e|_{T_i}$ and $C_i = \partial E/\partial T_i|_{T_e}$), from the MD, and show (for one of these hydrogen cases) that it can be understood from straightforward modeling. Additional predictions made with a quantum screened Coulomb model and with orbital-free density-functional theory indicate that these effects from time-varying potential energy should be noticeable for true quantum Coulomb hydrogen plasmas in these conditions as well.

(ii) Despite this success, we see that the kinetic ion temperature [30] and the configurational ion temperature [31] disagree, in that the instantaneous static structure of the ions is *not* that as expected for plasmas with T_i as defined by the ion velocity distribution function. Rather, it is reminiscent of a plasma with a somewhat lower T_i. Nevertheless, the analysis in (i) succeeds because the derivatives C_e and C_i are relatively insensitive to the differences in temperatures, i.e., E is linear over wide ranges of T_e and T_i.

(iii) We determine the instantaneous ion velocity distribution in the MD during temperature relaxation and quantify its departure from the equilibrium Maxwell-Boltzmann distribution. While this deviation does slightly affect the Lenard-Balescu prediction for temperature relaxation, explicit calculations using a polynomial expansion show that it should not significantly alter the equilibration rates (at least within the

weak-coupling approximation inherent in the Lenard-Balescu theory).

(iv) Most importantly, we quantify the energy relaxation rate in MD by decomposing the total energy into species-dependent pieces $E = E_i + E_e$ in which the electron-ion potential energy V_{ei} is shared equally between the species [21]. It is shown that dE_i/dt $(=-dE_e/dt)$ is far closer to the FGR predictions than to the CM predictions, in stark contrast to expectations.

The remainder of this paper is organized as follows. Section II presents our MD methodology, including a discussion of the multiple methods we use to initialize our 2T simulations. Section III contains a discussion of the perturbative treatment of the Lenard-Balescu equation used to predict the instantaneous time rates of change of electron and ion temperatures; here we focus on computational issues specific to predictions in the CM regime. A presentation of the results of our MD simulations and the comparison to the theoretical predictions (FGR and CM LB theory) appears in Sec. IV; this includes a discussion of the sizable effects of time-dependent potential energy, a study of the (negligible) effects of non-Maxwellian velocity distributions, and a discussion of possible reasons for the greatly reduced effect of coupled modes as compared to predictions [20]. We summarize in Sec. V.

II. MOLECULAR DYNAMICS SIMULATIONS

Coupled-mode temperature equilibration includes the possibility of nondegenerate electrons, making classical MD simulations a useful comparator. We employ the ddcMD code [32] with the particle-particle–particle-mesh method [33] for large-scale charged-particle simulations [34]. We mostly consider a subset of hydrogen cases studied by Vorberger and Gericke [20], $\rho = 10^{26}$ cm^{-3}, $T_i = 10^5$ K, and $T_e = 10^7$ to 5×10^8 K. The associated MD time steps range from 5×10^{-6} to 1×10^{-6} fs. Most simulations include 5.12×10^5 hydrogen atoms, but the first case is studied using 4.096×10^6 hydrogen atoms. This improves statistical sampling and reduces noise in the final results.

Even for nondegenerate electrons, the attractive electron-ion interaction requires some accommodation of quantum effects. Accordingly, we use the Dunn-Broyles diffractive QSP [27]. We include the two-body repulsive exchange piece introduced by Minoo *et al.* [28]. This prescription is used in the early temperature equilibration work of Hansen and McDonald [10] and much of our work on this subject [11,13]. It is an extension of the potentials (designed to reproduce quantum equilibrium pair correlations using classical particles) to a nonequilibrium situation. The potentials are parametrized for some desired target ion and electron temperatures $T_i^{\rm targ} \neq T_e^{\rm targ}$. The results for species α and β are then

$$V_{\alpha\beta}(r,T) = \frac{Z_\alpha Z_\beta e^2}{r}\left[1 - \exp\left(\frac{-2\pi r}{\Lambda_{\alpha\beta}}\right)\right] + k_B T \ln(2) \exp\left(\frac{-4\pi \ln(2) r^2}{\Lambda_{\alpha\beta}^2}\right)\delta_{\alpha e}\delta_{\beta e}, \quad (2)$$

where $\mu_{\alpha\beta} = m_\alpha m_\beta/(m_\alpha + m_\beta)$ and k_B is Boltzmann's constant. The QSP is dependent on temperatures through the de Broglie wavelength $\Lambda_{\alpha\beta} = \sqrt{2\pi\hbar^2/\mu_{\alpha\beta}k_B T^{\rm QSP}}$. (The temperature $T^{\rm QSP}$ is taken to be $T_i^{\rm targ}$ when α and β are both ions and simply $T_e^{\rm targ}$ if either is an electron.) In practice, these potential parameters are held constant at target values during a simulation even as the instantaneous temperatures vary widely with time. The time-independent Hamiltonian then ensures energy conservation for microcanonical simulations. Although this prescription is not in keeping with the behavior of true quantum electron wave packets as the electrons are cooled or heated, our aim in this work is simply to evaluate and critique the use of various theories in predicting T equilibration for systems with a *fixed* set of interaction potentials [35]. This was exactly the approach adopted in Ref. [11] as well.

Despite the well-defined Hamiltonian, a unique definition or preparation of a nonequilibrium two-temperature system may not always be feasible; specification of the effective temperatures leaves many degrees of freedom unconstrained. Practically, when constant particle number, volume, and energy (*NVE*) microcanonical simulations are allowed to evolve freely for a sufficient time, systems of a particular total energy E can often be found that pass through a desired target state $T_e^{\rm targ} \neq T_i^{\rm targ}$. This state can be considered unique as long as other out-of-equilibrium degrees of freedom set by the initial conditions have relaxed much faster than the global temperature difference. For example, intraspecies velocity equilibration can be much faster than electron-ion interspecies. This gives an effectively unique two-temperature state in weakly coupled cases. However, when the potential energy is substantial, differences between the configurational temperature [31] and the kinetic values [30] may exist and be relevant. In particular, the CM regime includes, by design, long-wavelength, underdamped, quasiharmonic ion acoustic waves (IAWs). Being underdamped, these modes would also be only weakly coupled to anything that might serve as a thermal bath. Hence, it is reasonable to suspect that different wavelength IAWs might evince different effective temperatures during equilibration and that structure factors and radial distribution functions will not correspond to those of a unique temperature. Normally, this might be ignored on phase space arguments (for small $|k|$, the number of modes is proportional to $|k|^3$ and the associated heat capacity is small), but the CM regime relies on having a sufficient number of slowly equilibrating degrees of freedom that the overall interspecies equilibration is affected.

Signatures of the potential energy are broadly visible in our CM temperature relaxation simulations. If a system is not carefully prepared, there is a prominent underdamped oscillation in the ion kinetic temperature at the start of the *NVE* evolution. Similar effects are seen when the electron temperature is abruptly altered [36]; the resulting change in the screened ion-ion potential switches the asymptotic pair distribution to some new $g_{ii}(r)$. Transient evolution away from the old stationary ion distribution towards the new one includes underdamped oscillations from IAWs. Such oscillations in our CM simulations are precisely compensated by variations in the ion potential energy $V_i \equiv V_{ii} + V_{ie}/2$, clearly showing the role of IAW collective modes. (Similar transients are not seen in the electron subsystem, which has much weaker coupling.) Yet another signature of the potential

energy is that the temperature relaxation rates are not equal and opposite $N_i \frac{dT_i}{dt} \neq -N_e \frac{dT_e}{dt}$, even after transient oscillations are mitigated. This will be discussed in more detail in Sec. IV.

Because of these complications, we consider three distinct approaches to MD sample preparation. In a few test cases, we start from near-stationary states subject to separate species-dependent thermostats, similar to past analyses. However, in our hydrogen CM cases, the ions require exceptionally strong thermostats to keep them cold. A Langevin thermostat [37] has the advantage of driving each species towards a Maxwell-Boltzmann velocity distribution. Unfortunately, the strong Langevin drag term has a time constant much less than a typical IAW period and so the IAWs are severely overdamped. In equilibrium, a quasiharmonic mode of wave number k should have an rms expected thermal amplitude given by equipartition of energy. However, given the overdamped ion dynamics, transient density perturbations will persist for times that scale as $1/k^2$, meaning that long-wavelength density fluctuations do not fully equilibrate during a simulation. In contrast, the Berendsen thermostat [38] simply scales all particle velocities of a given species so that their total kinetic energy is instantaneously related to the thermostat, $K \equiv \frac{3}{2} k_B T$. In this case, quasiharmonic oscillations are largely undamped by the thermostat and long-wavelength density fluctuations are left to equilibrate by means of weak intrinsic anharmonicities. This will give rise to different transient IAW behavior as the system relaxes. In addition, we prepare the most extreme two-temperature state possible so as to maximize the time for transient artifacts to decay. Systems are started with the ions in a simple cubic lattice, frozen in place at $T_i = 0$, i.e., all long-wavelength IAWs are initialized with exactly zero amplitude. The electrons are then equilibrated in a microcanonical MD simulation. Each initial state is characterized by its total energy E and is rigorously defined as part of a constrained equilibrium ensemble. Once the ions are released, we expect monotonic and continuous temperature relaxation with time. In particular, the family of instantaneous equilibrating states can be completely characterized by any two of the variables E, T_e, and T_i. This is akin to having an effective two-temperature thermodynamic potential $E(T_e, T_i)$, which can then be used to compute derivatives by finite differencing across different microcanonical simulations. This last preparation method is used for the majority of the simulations because of this advantage.

For example, a hydrogen case with $n = 10^{26}$ cm^{-3}, $T_p = 10^5$ K, and $T_e = 10^7$ K has been tested with all three preparation methods; all three give similar results. The total energy is tuned for each system until their electron temperatures are the same to within 0.1% when the target T_i is reached. The residual oscillations in $T_i(t)$ differ slightly in their magnitudes at the target conditions, but dT_i/dt can be measured across approximately one oscillation period to minimize any dependence on that amplitude. With that approach, the total potential energies at target are equal among the different preparation methods to within 0.1 eV/hydrogen atom (per hydrogen, per proton, or, equivalently, per electron) and the measured dT_i/dt are 5.45, 5.45, and 5.48 eV/fs for lattice, Langevin, and Berendsen initial configurations, respectively. Thus any possible long-lived differences in IAW amplitudes in the CM regime seem to have no effect on the potential energy of the system or the overall equilibration rates.

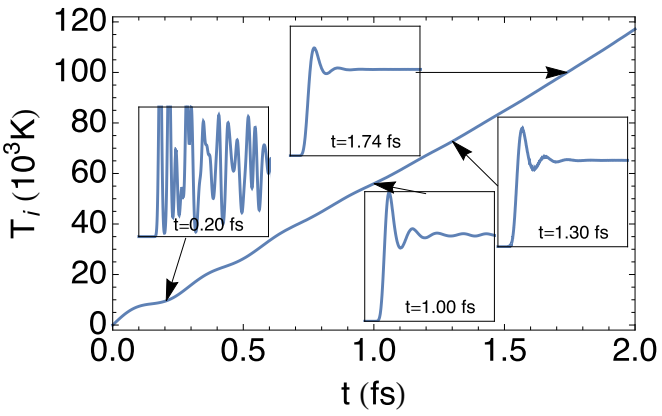

FIG. 1. Effective proton temperature $T_i = \frac{2}{3}\langle E_i^{\rm kin}\rangle$ versus time for a single *NVE* run of 8.192×10^5 particles (protons plus electrons). Oscillations in T_i correspond to underdamped transient relaxations in the ion-ion radial distribution function. Insets show the pair distribution function $g_{ii}(r,t)$, showing signs of crystalline order at early times. Long-range correlations are lost within 1.5 fs. The last inset shows the target conditions for this case, $T_p = 10^5$ K and $T_e = 10^7$ K, which occur at $t = 1.74$ fs.

A typical result for the lattice preparation procedure is shown in Fig. 1 for the ion temperature and for a series of ion-ion pair correlation functions $g_{ii}(r)$. At $t = 0$, the constraint on the ions is released and the ion temperature quickly begins to rise. Simultaneously, there are long-period transient oscillations initially visible in T_i. The initial lattice structure is lost well before the target condition of $T_i = 8.6$ eV ($\sim 10^5$ K) is reached in Fig. 1. By that time, the remnants of the long-period oscillations are also only of order ± 5 meV. In practice, $T_i(t)$ at this time is closely linear plus a sinusoidal component; the slope at the target is thus rendered insensitive to any long-period transient by making a linear fit over at least a complete cycle. Additionally, we note that the detailed shape of $g_{ii}(r)$ for times after the transient behavior has subsided is almost completely independent of the sample preparation scheme. In this sense, the nonadiabatic effects manifest in $g_{ii}(r)$ that we discuss later (in Sec. IV B) are also not the result of transient effects and are therefore representative of uniquely defined states.

For nonequilibrium plasmas, temperature relaxation is directly related to the underlying heat flow only in the weak-coupling limit. In the CM cases we study, $\Gamma_{ii} = 12.5$ ($= \frac{Z^2 e^2}{k_B T_i R}$, where $R = [\frac{3n}{4\pi}]^{1/3}$ is the average nearest-neighbor distance between ions) and the evolving potential energy is comparatively large. This evolution is associated with observed asymmetric temperature changes $N_i k_B dT_i/dt \neq -N_e k_B dT_e/dt$. To better quantify this, we will expand the MD analysis to include estimates of $(\frac{\partial V}{\partial T_i})_{T_e}$ and $(\frac{\partial V}{\partial T_e})_{T_i}$, analogous to a two-temperature excess heat capacity.

A single *NVE* simulation can only be used to compute dV/dt [or the gradient along the prescribed temperature trajectory $\vec{\nabla} V \cdot (dT_i/dt, dT_e/dt)^{\intercal}$]. Other derivatives in T_e and T_i space require cross comparison of different microcanonical ensembles. Figure 2 shows the temperature histories of three

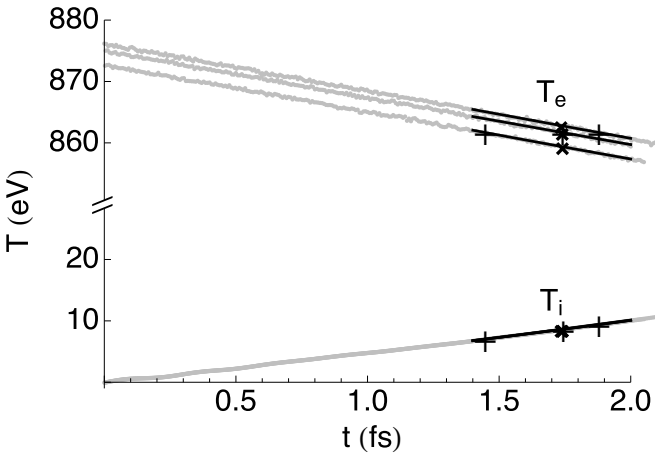

FIG. 2. Temperature histories are shown in light gray for three separate microcanonical MD simulations differing in total energy by a few eV per electron-ion pair. The temperature curves appear noisy because of intrinsic short-time fluctuations that are easily averaged over. Linear least-squares fits to portions of the time series are shown as black lines; dT/dt is computed analytically from these fits. The fitted curves each reach the target ion temperature ($T_p = 10^5$ K) at times marked by $\times$. They reach the target electron temperature ($T_e = 10^7$ K) at times marked with $+$. By design, these times coincide for the middle microcanonical system.

separate microcanonical simulations, spanning a range in E of about 4 eV/hydrogen atom. Each system is prepared with a lattice of ions at zero temperature; given the different total energies, the initial electron temperatures are well separated among the three systems. The middle T_e curve corresponds to the unique system total energy for which T_e and T_i both reach their respective target values at essentially equal times. The adjacent curves approximately cover some range $T_e(t=0)-\Delta$ to $T_e(t=0)+\Delta$. Since the change to each system is small $\Delta \ll T_e - T_i$, the relaxation rates dT_e/dt are nearly equal for the three runs and the curves are nearly parallel. Similarly, because the $T_i(t=0)$ initially coincide, all three ion temperature curves are nearly indistinguishable.

As discussed above, a linear least-squares fit is made to each temperature series $T(t)$ to suppress any transient oscillations; this is shown in Fig. 2 with short segments in black. We analytically obtain dT/dt at the target conditions from these fits. The symbols $\times$ and $+$ in Fig. 2 also mark the times along each fitted curve when the target temperature value is reached for ions or electrons, respectively. The instantaneous states at the marked points can then be used to compute temperature-dependent derivatives. Using the $\times$ points, we would obtain $E(T_i = 10^5\ \mathrm{K}, T_e)$ at three distinct T_e, while the $+$ points give $E(T_i, T_e = 10^7\ \mathrm{K})$ at three values of T_i. In practice, $E(T_i, T_e)$ is linear in T_e and T_i (and vice versa) for a family of instantaneous states over a small range of energies $[E-\Delta; E+\Delta]$, for Δ of order 1 eV per hydrogen atom. Thus, we apply another linear least-squares fit to $E(T_i)|_{T_e=10^7}$ or $E(T_e)|_{T_i=10^5}$ for multiple microcanonical systems within ± 1 eV/hydrogen atom. We then compute $\partial E/\partial T$ analytically. Since the kinetic energy component satisfies $K \equiv \frac{3}{2}k_B T$, the resulting derivatives also give estimates for $(\frac{\partial V}{\partial T_i})_{T_e}$ and $(\frac{\partial V}{\partial T_e})_{T_i}$.

III. LENARD-BALESCU THEORY

To analyze our MD results, as well as to exercise and test existing theories of the CM effect in T equilibration, we employ the generalized Lenard-Balescu (GLB) theory [16] outlined in detail in Ref. [8]. In this approach, the time rate of change of the ion temperature dT_i/dt in a 2T plasma is related via the fluctuation-dissipation theorem to the density response functions of the individual species. For the case of two species, electrons and ions, the result is [8]

$$\frac{dT_i}{dt} = -\frac{\hbar}{3\pi^3 n_\alpha}\int_0^\infty k^2 dk \int_0^\infty \omega\, d\omega \left[\frac{v_{ei}(k)}{D(k,\omega)}\right]^2 \times[1-G_{ei}(k,\omega)]\left[N\left(\frac{\hbar\omega}{2k_B T_i}\right) - N\left(\frac{\hbar\omega}{2k_B T_e}\right)\right] \times \mathrm{Im}\chi_e^0(k,\omega)\mathrm{Im}\chi_i^0(k,\omega), \quad (3)$$

where $D(k,\omega)$ is the two-species dielectric function

$$D = \left[1 - v_{ee}(1-G_{ee})\chi_e^0\right]\left[1 - v_{ii}(1-G_{ii})\chi_i^0\right] - v_{ei}^2(1-G_{ei})(1-G_{ie})\chi_e^0\chi_i^0, \quad (4)$$

involving the interparticle interactions v, free-particle density response functions χ^0, and local-field corrections (LFCs) G. Here $N(x)$ is a statistical factor arising from the fluctuation-dissipation theorem and is equal to $\coth(x)$ for fermions and $1/x$ for classical particles [39]. The response functions and LFCs are defined by the equation

$$\delta n_\alpha = \delta n_\alpha^0 + \chi_\alpha^0 \sum_\beta v_{\alpha\beta}[1-G_{\alpha\beta}]\delta n_\beta, \quad (5)$$

where the argument of each quantity is (k,ω). Here δn_α^0 are the density fluctuations in the absence of interactions, while δn_α are the density fluctuations in the presence of interactions [8,39], with species indexed by α and β.

Equation (5) expresses the self-consistent rearrangement of charge resulting from screening in the multicomponent plasma; if the LFCs ($G_{\alpha\beta}$) are set to zero, this is the random-phase approximation (RPA). The treatment of Eq. (3) with LFCs set to zero is equivalent to the Lenard-Balescu theory of T equilibration used in Refs. [7,20,21,23]. This is the theory we use to compare to MD for our hydrogen cases where QSPs have been used. For the like-charge Coulomb cases, it is essential for us to use nonzero LFCs (particularly G_{ei}) in order for the integral over k in Eq. (3) to be finite for large k [8]. These implementations of the GLB theory are identical to those we made in an earlier work [11].

The free-particle response functions χ^0 appearing in Eqs. (3)–(5) are the usual ones [39],

$$\chi_\alpha^0(k,\omega) = \lim_{\eta\to 0^+}\left[2\sum_{\mathbf{k}'}\frac{f_\alpha(\mathbf{k}'+\mathbf{k}) - f_\alpha(\mathbf{k}')}{\frac{\hbar^2(\mathbf{k}'+\mathbf{k})^2}{2m_\alpha} - \frac{\hbar^2 k'^2}{2m_\alpha} - \hbar\omega - i\eta}\right], \quad (6)$$

where $f_\alpha(\mathbf{k})$ is the occupation number for particles of energy $\hbar^2k^2/2m_\alpha$ at the temperature T_α. For our practical implementation for quantum particles, we use the Padé approximant fits for χ^0 appearing in Ref. [40]; for classical particles, we use the analytic expressions found in Ref. [41]. Since we have shown in the past [11] that the inclusion of (static, in that case) LFCs does not improve agreement with MD for T-equilibration rates

for hydrogen plasmas as modeled with QSPs, we set $G_{\alpha\beta} = 0$ in the remainder of this work.

As discussed in numerous works (e.g., Refs. [7,8,11]), the expression (3) reduces to that of far simpler expressions in many situations of interest. First, if the ions are taken to be much more massive than the electrons, as is physically the case, *and* the conditions are *not* those described by Eq. (1) [20], the f-sum rule for ions can be used to perform the ω integral analytically by evaluating the electron quantities at $\omega \approx 0$. This is strictly correct when coupled modes are neglected and arises from the fact that the plasma frequency of electrons far exceeds that of the ions, leading to the FGR result [4,20]. This FGR expression, now a single integral over k [see, for instance, Eq. (12) in Ref. [8]], can then be massaged into the familiar Landau-Spitzer equilibration rate in the limit of weak plasma coupling [8]:

$$\frac{dT_i}{dt} = \frac{T_e - T_i}{\tau_{ei}}, \tag{7}$$

where

$$\frac{1}{\tau_{ei}} = \frac{8\sqrt{2\pi}\, n_i Z_i^2 e^4}{3 m_e m_i}\left[\frac{k_B T_e}{m_e} + \frac{k_B T_i}{m_i}\right]^{-3/2} \ln\lambda_{ei}, \tag{8}$$

and $\ln\lambda_{ei} = \ln(b_{\max}/b_{\min})$, as described above. Here the screening length $b_{\max}$ arises from the small-k part of the dielectric function D in Eq. (3). The $b_{\min}$ comes from either the large-k part of $\mathrm{Im}\chi_e^0$ (the de Broglie wavelength in the quantum Coulomb case) or the large-k part of $1 - G_{ei}$ (the classical turning point in the classical Coulomb case) [8]. For the classical QSP case, $b_{\min}$ arises from the large-k behavior of $v_{ei}(k)$ (the de Broglie wavelength) [11]. The expressions (7) and (8), as well as the full GLB expression (3), respect kinetic energy conservation, consistent with the assumption of weak plasma coupling.

If coupled modes are important, as is predicted to be the case for two-component plasmas satisfying Eq. (1), a reduction of Eq. (3) to a Landau-Spitzer-like expression is not possible [23]. However, as long as the plasma is not too strongly coupled, it is expected that the full double-integral expression (3) should still produce reliable predictions and indeed it is essentially this theory that was used by Vorberger and Gericke to derive the regime indicated by Eq. (1). In Ref. [20] these authors emphasized that the correct inclusion of coupled modes (in the form of ion acoustic waves) in T equilibration within the Lenard-Balescu theory is quite numerically challenging, because the structure of the ω integrand possesses peaks that are infinitesimally sharp at small k, where the effect is most important. This can be seen most easily by examining the structure of the energy loss function $\mathcal{L}(k,\omega) \equiv \mathrm{Im}[1/D(k,\omega)] = -\mathrm{Im}[D]/([\mathrm{Im}D]^2 + [\mathrm{Re}D]^2)$. If v_{ei} is set to zero, this function has separate electron and ion plasmon peaks at the respective plasma frequencies, when $\mathrm{Re}D = 0$ and $\mathrm{Im}D$ is very small. However, when $v_{ei} \neq 0$, the low-k portion of the ion plasmon sharpens while losing its intensity and moves to much lower frequency, ceasing to contribute substantively to the dT_i/dt integral.

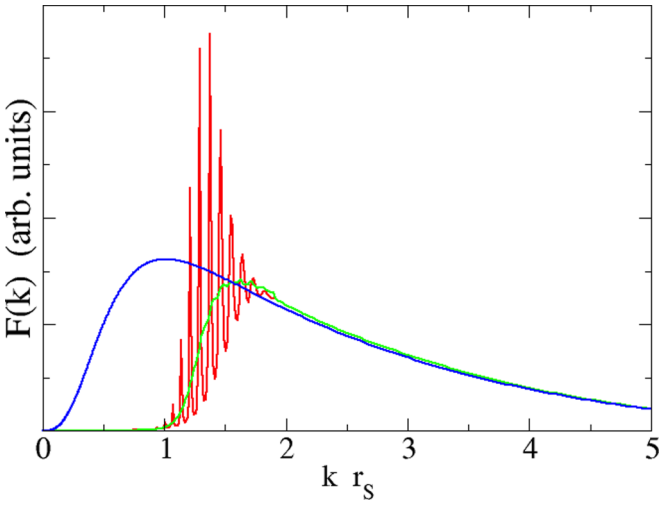

FIG. 3. The k integrands $F(k)$ of various Lenard-Balescu expressions for the equilibration rate for the quantum hydrogen plasma with $n = 1.0 \times 10^{26}$ cm^{-3}, $T_i = 10^5$ K, and $T_e = 10^7$ K. The red curve shows $F(k)$ computed by Eq. (3), using the naive evaluation scheme outlined in Ref. [11]; the green curve shows $F(k)$ from Eq. (3), but computed with the pole-correction scheme outlined here; the blue curve shows $F(k)$ from the FGR expression of Eq. (10). The integrals under the two CM Lenard-Balescu $F(k)$ curves shown here (red and green) are equal to within 1% for this case.

We illustrate the contributions to this integral by examining the k integrand $F(k)$, defined such that

$$\frac{dT_i}{dt} = \int_0^\infty F(k)dk, \tag{9}$$

i.e., the k-dependent function that results from performing the ω integral in Eq. (3). Figure 3 shows $F(k)$ computed for the (quantum Coulomb) hydrogen plasma (here, taking all $G_{\alpha\beta} = 0$) with $n = 1.0 \times 10^{26}$ cm^{-3}, $T_i = 10^5$ K, and $T_e = 10^7$ K. The blue curve is the result of the FGR theory, which assumes no coupled modes and arises from Eq. (12) in Ref. [8], reproduced here as

$$\frac{dT_i}{dt} = \frac{(T_i - T_e)}{3\pi^2 m_i}\int_0^\infty dk\, k^4 \left[\frac{v_{ei}(k)}{\epsilon_e(k,0)}\right]^2 \left(\frac{\partial\, \mathrm{Im}\chi_e^0}{\partial\omega}\right)_{\omega=0}, \tag{10}$$

where ϵ_e is the one-component RPA plasma dielectric function of the electrons ($\epsilon_e = 1 - v_{ee}\chi_e^0$). The red curve shows $F(k)$ computed with Eq. (3) using the numerical prescription outlined in Ref. [11], in which a logarithmic ω mesh is used to compute the ω integral, but no special attention is paid to ensuring that the ω poles for small k are resolved properly [42]. The sharp peaks and valleys in $F(k)$ at the smaller k values arise from the improper treatment of the pole for which D is very close to zero; as k is changed, the pole alternately moves close to and farther from the nearest ω-mesh point, resulting in inaccurate integration. This can be corrected by treating the pole explicitly [20]. In our simple treatment here, we approximate this feature as a Lorentzian peak in the loss function $L(x) = \frac{1}{\pi}\frac{\Gamma/2}{(x-x_0)^2+(\Gamma/2)^2}$. While $\mathcal{L}(k,\omega)$ does not appear directly in Eq. (3), multiplying and dividing by $\mathrm{Im}D$ allows us

to rewrite Eq. (3) in the following way:

$$\frac{dT_i}{dt} \propto \int_0^\infty v_{ei}^2(k)k^2dk \times \int_0^\infty \frac{\omega d\omega}{|D(k,\omega)|^2}\Delta N(\omega)\mathrm{Im}\chi_e^0(k,\omega)\mathrm{Im}\chi_i^0(k,\omega) \equiv \int_0^\infty v_{ei}^2(k)k^2dk\, I(k),$$

where

$$I(k) = \int_0^\infty \frac{\omega\, d\omega\, \Delta N(\omega)\mathrm{Im}\epsilon_e\mathrm{Im}\epsilon_i}{|D(k,\omega)|^2} = \int_0^\infty \frac{\omega\, d\omega\, \Delta N(\omega)\mathrm{Im}\epsilon_e\mathrm{Im}\epsilon_i}{\mathrm{Im}D}\left[\frac{\mathrm{Im}D}{|D(k,\omega)|^2}\right] \equiv \int_0^\infty d\omega\, R(k,\omega)\mathcal{L}(k,\omega).$$

Here ΔN is the difference of statistical factors appearing in Eq. (3) and the individual species dielectric functions are defined by

$$\epsilon_e = 1 - v_{ee}\chi_e^0, \quad \epsilon_i = 1 - v_{ii}\chi_i^0.$$

In addition, $R(k,\omega)$ is the ω integrand of Eq. (3), but with the loss function factored out. Further, $\mathcal{L}(k,\omega) \to L(\omega-\omega_0) \sim \delta(\omega-\omega_0)$ when $\mathrm{Re}[D]$ goes through 0 and $\mathrm{Im}[D] \to 0$. Thus,

$$I(k) \to \frac{\pi}{A}R(k,\omega_0),$$

when $\mathrm{Re}[D] \sim A(\omega-\omega_0)$. The width of the Lorentzian is $\mathrm{Im}D(\omega_0)/A$ and can be compared to the quadrature mesh size $\Delta\omega$. We then take the corrected integral to be (uncorrected integral on the ω mesh) − (integral of the approximated form on the ω mesh) + (analytically derived correction). This strategy produces the green curve in Fig. 3. Note that this curve still possesses peaks and valleys at locations identical to those of the red curve, but their magnitudes are greatly suppressed. The remaining bumps are an artifact of the approximation, $\mathcal{L}(k,\omega) \to L(\omega-\omega_0)$; a better representation of the true asymmetrically broadened ion acoustic wave peak yields still smoother results [20,23]. However, we note that the final integral $\int_0^\infty F(k)dk$ is equal to within 0.1% for red and green curves. Thus, the main feature of coupled modes, the extinguishing of the small-k contributions to dT_i/dt (relative to that of the FGR theory; see Fig. 3) [20], is captured even for a naive evaluation of Eq. (3). This is less true as T_e is raised and the ratio T_e/T_i is increased; we have noted up to 10% deviations in some cases, when using the naive evaluation. Therefore, all of the results we present here make use of the pole-correction strategy above; we will see below that they agree quantitatively with the predictions of Ref. [20] for quantum Coulomb hydrogen plasmas.

Since we are (a) reinvestigating prior predictions for quantum plasmas and (b) comparing to the results of our classical MD studies with QSPs, we carry forth the above GLB prescription in two modes: (i) with quantum statistics and quantum response functions together with the bare Coulomb interaction and (ii) with classical statistics and classical response functions together with the QSPs. This is in the spirit of our earlier MD and theory work on T equilibration not in the CM regime [11], where we found that the use of Dunn-Broyles QSPs and classical statistics substantively reduced the equilibration rates relative to the quantum Coulomb predictions [43]. Because our aim in this work is to use MD to validate theories that have predicted the CM effect in T equilibration, it is crucial for us to separate possible reductions in rates resulting from the use of classical MD and QSPs from the actual coupled-mode effect itself. In this sense, the classical QSP system is to be thought of as a theoretical surrogate in which the CM effect is studied. If agreement between classical QSP MD and classical QSP Lenard-Balescu theory is demonstrated, our confidence in the quantum Lenard-Balescu predictions of the CM effect for real plasmas is strengthened.

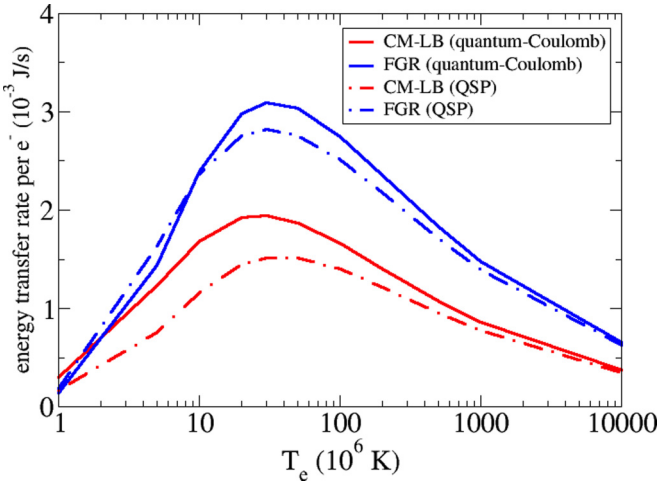

FIG. 4. Instantaneous energy transfer rate per e^- for hydrogen plasmas with $n = 10^{26}$ cm^{-3} and $T_i = 10^5$ K, as a function of T_e. The solid red curve shows the quantum Coulomb prediction using the CM Lenard-Balescu approach; the solid blue curve shows the quantum Coulomb prediction with the FGR prescription; the dot-dashed red curve shows the classical QSP prediction using the CM Lenard-Balescu approach; the dot-dashed blue curve shows the classical QSP prediction with the FGR prescription.

IV. RESULTS AND DISCUSSION

A. Molecular dynamics results for the Vorberger-Gericke hydrogen plasmas ($n = 10^{26}$ cm^{-3}, $T_i = 10^5$ K, and 10^7 K $< T_e <$ 10^9 K)

We report T equilibration for the family of hydrogen plasmas with density $n = 10^{26}$ cm^{-3}, $T_i = 10^5$ K, and T_e between 10^6 and 5×10^8 K. These plasmas were considered in Ref. [20] using the LB theory and were predicted to equilibrate at rates substantially slower than those as predicted by the FGR approach and a variant of the Landau-Spitzer theory.

First we discuss our version of the LB predictions for these cases. The solid curves of Fig. 4 display the energy transfer rate per electron, as a function of T_e, computed in two ways: (i) a solid red line shows the CM Lenard-Balescu theory [Eq. (3) with zero LFCs], and (ii) a solid blue line shows the FGR theory [Eq. (10)]. Both curves result from the quantum Coulomb evaluation of these equations. These curves compare very favorably with the corresponding curves in Fig. 4 of Ref. [20]. The only notable discrepancy is at low

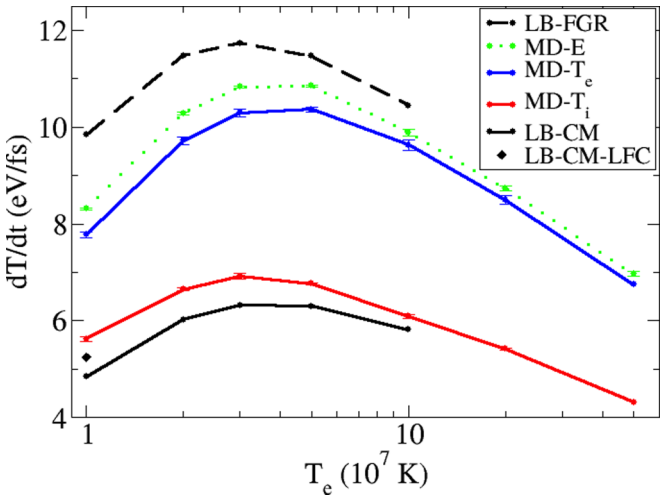

FIG. 5. Instantaneous dT/dt calculated from the classical QSP Lenard-Balescu approach and extracted from MD using the identical QSPs for hydrogen plasmas with $n = 10^{26}$ cm^{-3}, $T_i = 10^5$ K, and T_e as shown on the x axis. The uppermost, thick, dashed black curve is for LB FGR theory and the lowest, thick, solid black curve is for the LB CM theory. The disconnected black point corresponds to a local-field-corrected LB CM calculation using two-temperature HNC. Only the ion-ion local-field correction is included. Red symbols with error bars and thin solid lines correspond to MD for dT_i/dt and blue symbols with error bars and thin dashed lines correspond to MD for $-dT_e/dt$. The green symbols with error bars and thin dotted lines show the MD results for the time rate of change of total energy, scaled by 2/3 from Table I to correspond to a temperature, i.e., $\frac{2}{3}dE_e/dt$ (see also Table II). (the relation $dE_i/dt = -dE_e/dt$ holds exactly).

T_e and is due to the fact that our FGR evaluation neglects electron degeneracy, unlike that of Ref. [20]. As indicated in the preceding section, our numerical treatment of the sharp low-k poles in the dielectric function of Eq. (3) is sufficiently accurate to agree with the more carefully resolved results of Ref. [20]. The dot-dashed curves of Fig. 4 show our calculations for the same plasmas, but for the classical QSP cases, assuming Dunn-Broyles diffractive terms [27] and Minoo *et al.* exchange contributions [28] evaluated at the electron temperatures T_e. These are the QSPs used for our classical MD studies for these plasmas, to be discussed directly below. The red dot-dashed curve is the CM LB result, while the blue dot-dashed curve is the FGR prediction. Note that for both curves, the energy transfer rates are substantially lower than those of the quantum Coulomb results plotted in Fig. 4. This reduction is very similar to that noted for the hydrogen cases studied in Ref. [11] when comparing quantum Coulomb to classical QSP Lenard-Balescu predictions (for the same choices of QSPs).

Figure 5 shows the predictions of Fig. 4 once again, but now expressed as $|dT/dt|$ for the species rather than as an energy transfer rate. Also displayed are our MD results obtained using the ion-lattice preparation method discussed in Sec. II. We extract these rates as in Fig. 2, by fitting the MD time series around the target conditions; they are therefore some effective time average of noisy MD dT_i/dt, $-dT_e/dt$, and dE/dt, respectively. We note that dT_i/dt from the MD is slightly higher than the prediction from the Lenard-

TABLE I. Temperature relaxation rates $|dT/dt|$. All units are eV/fs. Here $E_i = 3/2kT_i + V_i$, with $V_i = V_{ei}/2 + V_{ii}$, and $|dE_i/dt| = |dE_e/dt|$. When the energy rate of change is plotted in Fig. 5, it is expressed as $\frac{2}{3}|dE/dt|$ to compare to temperature derivatives.

T_e (K)	MD ion	MD electron	MD E	LB CM	LB FGR
1×10^7	5.63 ± 0.05	7.78 ± 0.06	12.46 ± 0.04	4.839	9.840
2×10^7	6.65 ± 0.03	9.72 ± 0.08	15.43 ± 0.05	6.027	11.475
3×10^7	6.92 ± 0.06	10.30 ± 0.08	16.25 ± 0.03	6.321	11.732
5×10^7	6.77 ± 0.02	10.37 ± 0.05	16.28 ± 0.04	6.305	11.474
1×10^8	6.09 ± 0.04	9.63 ± 0.11	14.83 ± 0.11	5.818	10.451
2×10^8	5.42 ± 0.02	8.49 ± 0.09	13.10 ± 0.07		
5×10^8	4.32	6.75	10.45 ± 0.08		

Balescu theory including coupled modes, while $-dT_e/dt$ is far higher still. The two MD temperature derivatives approach equality for more weakly coupled plasmas; indeed, essentially symmetric relaxations ($dT_e/dt = -dT_i/dt$) were noted in earlier work on hydrogen plasmas [8,9,11–13]. In our cases here, however, the ions are sufficiently cold that such an asymmetric temperature relaxation is expected [7,21,23]. This results from the sizable potential energy in the (somewhat strongly correlated) screened ions, which diminishes as the ions are heated. The effect on dT_e/dt and dT_i/dt is simple to analyze using conservation of energy, within the rubric of the 2T hypothesis we have invoked.

Since, after initial preparation, our MD simulations represent closed systems that evolve microcanonically, the total system energy E is conserved and we have

$$E(T_e,T_i) = K_e(T_e) + K_i(T_i) + V(T_e,T_i), \tag{11}$$

$$\frac{dE}{dt} = 0 = \left[\frac{3}{2}N_e + \left(\frac{\partial V}{\partial T_e}\right)_{T_i}\right]\frac{dT_e}{dt} + \left[\frac{3}{2}N_i + \left(\frac{\partial V}{\partial T_i}\right)_{T_e}\right]\frac{dT_i}{dt}, \tag{12}$$

where K_e and K_i are electron and ion kinetic energies and are functions only of their respective temperatures and V is the total system potential energy, which we assume to be a unique

TABLE II. Excess heat capacity in eV/fs. Species temperature is defined by $3/2kT$, which is equivalent to the kinetic energy; the ideal heat capacity is 3/2.

T_e (K)	$dV/dT_p\|_{T_e}$	$dV/dT_e\|_{T_p}$
1×10^7	0.629 ± 0.03	0.027 ± 0.02
2×10^7	0.698 ± 0.03	-0.027 ± 0.02
3×10^7	0.765 ± 0.05	0.00 ± 0.03
5×10^7	0.810 ± 0.04	0.00 ± 0.03
1×10^8	0.895 ± 0.04	0.016 ± 0.02
2×10^8	0.915 ± 0.04	0.12 ± 0.08
5×10^8	0.832 ± 0.06	-0.026 ± 0.03

function of T_e and T_i [44]. Equating the two summands gives

$$\left[\frac{3}{2}N_e+\left(\frac{\partial V}{\partial T_e}\right)_{T_i}\right]\frac{dT_e}{dt}=-\left[\frac{3}{2}N_i+\left(\frac{\partial V}{\partial T_i}\right)_{T_e}\right]\frac{dT_i}{dt}, \quad (13)$$

which leads to a prediction for the asymmetry in the T derivatives:

$$\frac{\left|\frac{dT_e}{dt}\right|}{\left|\frac{dT_i}{dt}\right|}=\frac{\left[\frac{3}{2}N_i+\left(\frac{\partial V}{\partial T_i}\right)_{T_e}\right]}{\left[\frac{3}{2}N_e+\left(\frac{\partial V}{\partial T_e}\right)_{T_i}\right]}. \quad (14)$$

For our hydrogen cases, $N_e=N_i$, and since the Lenard-Balescu theory conserves only kinetic energy, our LB prediction (black curve in Fig. 5) is consistent with the $V=0$ version of Eq. (14),

$$\frac{\left|\frac{dT_e}{dt}\right|_{\rm LB}}{\left|\frac{dT_i}{dt}\right|_{\rm LB}}=\frac{N_i}{N_e}=1. \quad (15)$$

The asymmetry in the T relaxation is due to the nonzero V and in particular to the specific derivatives of V that appear in Eq. (14).

Before we discuss these potential energy derivatives further, we note that our MD results for energy relaxation $dE_i/dt=-dE_e/dt$ are far closer to the FGR predictions than to those of the Lenard-Balescu theory when coupled modes are included. This can be seen in Fig. 5, in which the dotted green line and circles display the MD values for $\frac{2}{3}dE_i/dt$ (with $k_B=1$), where the species-specific internal energies are defined by Eq. (16) exactly as in Ref. [21]:

$$E_i=K_i+V_{ii}+\tfrac{1}{2}V_{ei}, \quad E_e=K_e+V_{ee}+\tfrac{1}{2}V_{ei}. \quad (16)$$

While the LB predictions (either CM or FGR) are only consistent with $E_i=K_i$ and $E_e=K_e$, it is reasonable to expect that the energy transfer rates might be well predicted by the LB theory, since the primary drivers for the energy exchange, Coulomb collisions, are included therein. Indeed, it is for this reason that the LB predictions of Ref. [20] were represented as energy transfer (rather than temperature equilibration) rates; those authors left open the possibility that nonideal specific heats would have to be included to relate the $dE_{e,i}/dt$ from the LB theory to the $dT_{e,i}/dt$, as they did subsequently in their work of Ref. [21]. However, our MD results for these cases clearly show the $dE_{e,i}/dt$ themselves to be in disagreement with the coupled-mode LB predictions. This is discussed further in Sec. IV C. We emphasize that these conclusions can only be drawn by making the proper comparisons: classical QSP LB theory vs classical QSP MD [11].

B. Elucidation of 2T equation of state for the $T_e=10^7$ K case

In this section we explore one of the particular cases studied above: $n=10^{26}$ cm^{-3}, $T_i=10^5$ K, and $T_e=10^7$ K; this system has intraspecies plasma coupling constants $\Gamma_{ee}\sim 0.125$ and $\Gamma_{ii}\sim 12.5$. To establish that the large discrepancies between dT_i/dt and $-dT_e/dt$ in the MD results, as shown in Fig. 5, can be accounted for by considering the $(\frac{\partial V}{\partial T_i})_{T_e}$ and $(\frac{\partial V}{\partial T_e})_{T_i}$ in Eq. (14), we extract these quantities independently using two approaches: (i) from additional molecular dynamics simulations and (ii) from (adiabatic and quasistatic) theoretical estimates. Regarding (i), potential energy derivatives at fixed T_e or T_i can be inferred from families of T-equilibration MD simulations performed at closely spaced initial conditions, as described in Sec. II. This produces the values $(\frac{\partial V}{\partial T_i})_{T_e}=0.586k_B/e^-$ and $(\frac{\partial V}{\partial T_e})_{T_i}=0.0328k_B/e^-$ for this case. Our values for $|dT_e/dt|$ and dT_i/dt are 7.92 and 5.59 eV/fs, respectively, giving a left-hand side of Eq. (14) of 1.42; plugging our values for $(\frac{\partial V}{\partial T_i})_{T_e}$ and $(\frac{\partial V}{\partial T_e})_{T_i}$ into the right-hand side gives 1.36.

Regarding the second (theoretical) approach, V can be computed from the three radial distribution functions $g_{ee}(r)$, $g_{ii}(r)$, and $g_{ei}(r)$, since the interparticle QSPs are two body in nature [45]:

$$V=\frac{n_{\rm tot}}{2}\sum_{\alpha,\beta}x_\alpha x_\beta\int d^3r\, g_{\alpha\beta}(r)v_{\alpha\beta}(r), \quad (17)$$

where α and β indicate species (e,i), $n_{\rm tot}=\sum_\alpha n_\alpha$, and $x_\alpha=n_\alpha/n_{\rm tot}$. We use a two-temperature variant [46] of the hypernetted-chain (HNC) approximation [47] to determine the $g_{\alpha\beta}(r)$ to be input into this expression. Here the equations have been generalized to include mass-weighted temperatures $T_{ij}=(m_jT_i+m_iT_j)/(m_i+m_j)$, which is roughly equal to T_e for this case. This approximation is valid for systems in which each species can be described by distinct Maxwellian distributions [48] and both the mass discrepancies ($m_e\ll m_i$) and temperature discrepancies ($T_e\gg T_i$) of the systems of interest in our work reinforce this assumption. With these HNC-derived $g_{\alpha\beta}(r)$ and Eq. (17) [49], V is determined at the nominal $T_i=10^5$ K and $T_e=10^7$ K. Repeating the whole calculation at $T_i+\delta T_i$ and $T_e+\delta T_e$ then produces $(\frac{\partial V}{\partial T_i})_{T_e}=0.5352k_B/e^-$ and $(\frac{\partial V}{\partial T_e})_{T_i}=0.009\,728k_B/e^-$. While $(\frac{\partial V}{\partial T_e})_{T_i}$ is rather different from that of the direct MD determination outlined above, $(\frac{\partial V}{\partial T_i})_{T_e}$ is quite similar; the smallness of $(\frac{\partial V}{\partial T_e})_{T_i}$ relative to 3/2 then results in the prediction $|\frac{dT_e}{dt}|/|\frac{dT_i}{dt}|=1.33$, once again slightly below the MD value of 1.42.

While the aforementioned theory-MD agreement is reasonable for $(\frac{\partial V}{\partial T_i})_{T_e}$ and $(\frac{\partial V}{\partial T_e})_{T_i}$, it is interesting to look directly at the $g_{\alpha\beta}(r)$ from the MD, since our HNC calculations of these quantities are necessarily somewhat approximate. Figure 6 shows g_{ee}, g_{ei}, and g_{ii} for the $n=10^{26}$ cm^{-3}, $T_i=10^5$ K, and $T_e=10^7$ K case. Solid lines show the results of our QSP MD, where the average over snapshots was performed over a duration small enough to render T_e and T_i determinations essentially instantaneous. The dashed lines show our HNC calculations for this case using the identical QSPs; these are the functions that we input into Eq. (17) to obtain our estimates of V for these conditions. Note that while g_{ee} and g_{ei} are in excellent agreement, g_{ii} is considerably more structured in our MD. At first blush, one might expect such a result, since the bare ion-ion plasma coupling is quite large here ($\sim$12.5), while T_e is possibly high enough to render the electrons nearly equivalent to a negative uniform compensating background that is incapable of affecting much in the way of screening. This last statement is borne out in Fig. 7, showing the evolution of the first peak in $g_{ii}(r)$ from MD; as T_e is raised from 10^7 K to 10^8 K, the behavior seems to asymptote to what we must assume is the $T_e\to\infty$ ion one-component plasma (OCP) result. However, since the $T_e=10^7$ K g_{ii} (MD) is

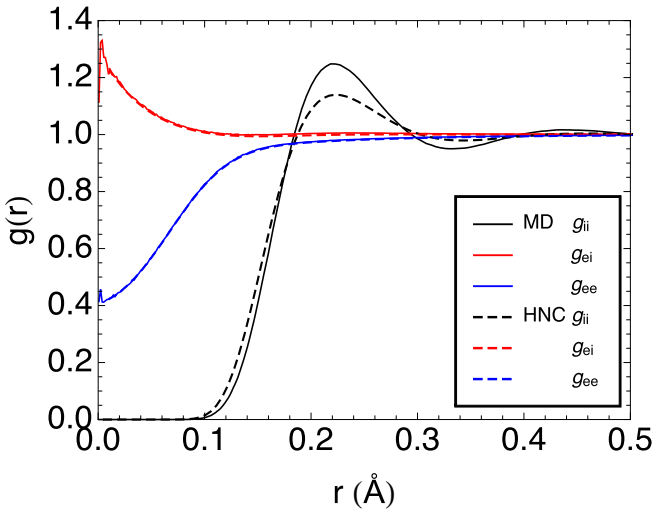

FIG. 6. Plots of $g(r)$ from MD and the HNC approximation for the $T_e = 10^7$ K case.

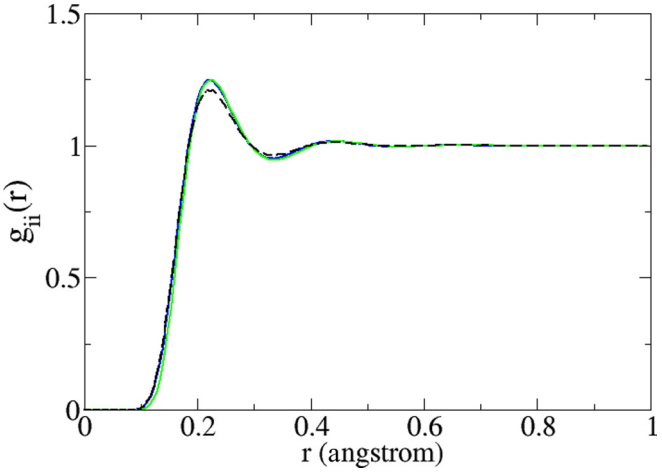

FIG. 8. Instantaneous MD ion-ion pair distribution function $g_{ii}(r)$ for the hydrogen plasma with $n = 10^{26}$ cm^{-3}, $T_i = 10^5$ K, and $T_e = 10^7$ K (solid blue curve, essentially obscured by the green curve), compared with the ion OCP $g_{ii}(r)$ for the identical n, but with $T_i = 6.777 \times 10^4$ K (solid green curve). Also shown is the MD result for the same plasma, but with the mass of the protons artificially increased by a factor of 8 (dashed black curve).

already much closer to the $T_e = 5 \times 10^8$ K g_{ii} (MD) than it is to the g_{ii} (HNC) shown in Fig. 6, it is possible that our HNC predictions of $g_{ii}(r)$ might be rather inaccurate. Two points are worth noting here. (i) The near independence of g_{ii} (from the MD) on T_e in this regime suggests that the ion OCP model is in fact a good one for g_{ii}; this in turn means that the consequences of the detailed assumptions inherent in the nonequilibrium 2T variant of HNC we employ (see Appendix A and the work of Ref. [46]) are minimized. (ii) The HNC approximation of the 1T (here equal to $T_{\rm ion}$) variety is known to work exceedingly well for the OCP when the plasma coupling is ∼12.5 and far greater. Thus, we can trust that the discrepancy between g_{ii} (MD) and g_{ii} (HNC) is likely not due to a failure of HNC for the chosen values of n and T_i.

We therefore explore the possibility that the actual ion-ion correlations in the MD for this case are not those of an ion OCP with $T_i = 10^5$ K. Figure 8 shows g_{ii} (MD) once again (solid blue curve), together with an ion OCP $g_{ii}(r)$ as computed with the HNC approximation, but at a lower $T_i = 6.777 \times 10^4$ K (solid green curve). They are nearly identical, suggesting that

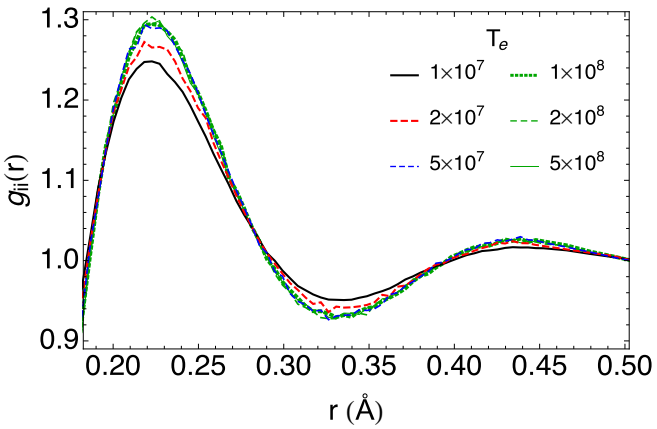

FIG. 7. Close-up of the ion-ion pair distribution functions for $T_i = 10^5$ K and a series of electron temperatures.

the ions in the nonequilibrium MD calculation are spatially correlated in a manner notably different from that expected from a system in thermal equilibrium at $T_i = 10^5$ K. Indeed, our nominal value of $T_i = 10^5$ K is computed from the ion kinetic energies. We thus find the kinetic temperature to be different from the configurational temperature here. While we have seen that this has only a modest affect on the analysis of time-varying potential energy in this regime (with regard to the various T derivatives of V) [50], we are open to the possibility that such a difference could alter an estimation of the energy exchange rate. As of this writing, we do not have a theoretical tool to assess this, nor do we have a detailed understanding of how, in practice, a sizable difference between kinetic and configurational temperatures could come about. To at least establish that this difference arises from nonadiabatic effects, we have conducted MD studies for this same plasma, but with the proton mass increased by a factor of 8 relative to its physical value. The results for $g_{ii}(r)$ are shown as the black dashed curve in Fig. 8. Note that this $m_i = 8m_p$ plasma is less structured than the $m_i = m_p$ plasma; HNC calculations for the ion OCP (not shown) at this density match the black dashed curve well when $T_{\rm config} \sim 7.5 \times 10^4$ K, intermediate between $T_{\rm kinetic}$ and $T_{\rm config}$ for the associated plasma with the physical ion mass. It is therefore clear that the fundamental source of $T_{\rm config} \neq T_{\rm kinetic}$ is the dynamics of the energy exchange process itself. This interesting subject awaits further study.

We have demonstrated that the asymmetric initial relaxations indicated in Figs. 2 and 5 result from the T_i dependence of the potential energy in our classical QSP MD simulations for hydrogen. This is not surprising, since T_i (10^5 K) is quite low for all of these cases, particularly for such a high density (10^{26} cm^{-3}). However, since these conclusions are based on a classical QSP model of hydrogen, it is natural to ask whether such an asymmetry would be present in a real hydrogen plasma in these conditions. We address this by adapting the above

theoretical estimate, pertaining to Eq. (17), to the quantum electron case by mapping onto an effective one-component (ion-only) Yukawa system as in the work of Ref. [45]. The HNC approximation is used once again to compute $g_{ii}(r)$, this time interacting via screened interactions determined from linear response. The electronic part of the free energy is taken from the fit of Tanaka and Ichimaru [51]. Details of our procedure are left to the Appendix. This produces potential energy derivatives that are broadly similar to those quoted above, $(\frac{\partial V}{\partial T_i})_{T_e} = 0.4351 k_B/e^-$ and $(\frac{\partial V}{\partial T_e})_{T_i} = 0.028\,68 k_B/e^-$, and derivatives of the total energy (including the quantum electron kinetic energy terms) of $(\frac{\partial E}{\partial T_i})_{T_e} = 1.7176 k_B/e^-$ and $(\frac{\partial E}{\partial T_e})_{T_i} = 1.4347 k_B/e^-$, indicating a ~20% asymmetry between $-dT_e/dt$ and dT_i/dt [52].

Orbital-free (OF) density-functional theory (DFT) [53–55] provides another way for us estimate the energetics of 2T quantum hydrogen plasmas. We employ a treatment that invokes the Born-Oppenheimer approximation, which decouples the electronic and nuclear motions. The nuclei evolve classically and the electronic contribution derives from a minimization of a quantum free-energy functional in terms of the full electron probability density. We employ a modified Thomas-Fermi-Dirac form that includes the Perrot finite-temperature kinetic-entropic contribution and a local-density exchange-correlation component. The Born-Oppenheimer dichotomy does not permit the direct examination of nonadiabatic processes such as electron-ion equilibration. However, since the OF DFT MD allows setting T_e and T_i independently for a given simulation, we can elicit the temperature dependence of the total internal energy within this adiabatic scheme. For these comparisons, we consider 432 H atoms (N_i) in a periodic box for trajectories of 10^4 time steps of length 0.012 fs. We have also tested convergence in atom number (128 to 1024), time step, and trajectory length and found variations in the total internal energy E and pressure of less than 1%. By using a range of closely spaced T_i for a fixed T_e, we find $(\frac{\partial E}{\partial T_i})_{T_e} = 2.07 \pm 0.2 k_B/e^-$ [56]. As in the above HNC estimates, the variation of E with T_i at fixed T_e is sizable. We therefore expect that a real hydrogen plasma under these conditions will also exhibit an initial asymmetric T relaxation.

As we mentioned in the Introduction, our main reason for studying out-of-equilibrium plasmas in this manner is to assess and improve upon models currently used in continuum simulations of, e.g., ICF [1,2]. In such simulations, equation of state (EOS) models are invoked that typically arise from single-temperature constructs that assume that all thermodynamic functions are derived from Helmholtz free energies of the form [57]

$$F(\rho,T) = E_0(\rho) + F_i(\rho,T) + F_e(\rho,T). \tag{18}$$

Here E_0 is the "cold" piece representing the density dependence of the energy of ions fixed in position (equal to zero for a low-density gas), F_i represents the free energy due to ionic motion (phonons in a solid and more general ionic excitations in a liquid), and F_e represents the free energy of electronic excitations. Implicit is the assumption that ionic and electronic excitations are decoupled; this neglects, for instance, any change in interionic forces that may occur when electrons are strongly excited. When electron-ion T splits are invoked in most ICF simulations [1], the following approximation is often made to construct a 2T free energy from the 1T free energy above [57]:

$$F_{2T}(\rho,T_i,T_e) \equiv E_0(\rho) + F_i(\rho,T_i) + F_e(\rho,T_e), \tag{19}$$

leading immediately to

$$E_{2T}(\rho,T_i,T_e) = E_0(\rho) + E_i(\rho,T_i) + E_e(\rho,T_e). \tag{20}$$

This assumption of Eq. (19) is only reasonable when the EOS itself is practically ideal gaslike. When T_e and T_i are very different and the material is somewhat strongly coupled, it is highly suspect.

Applying this to T equilibration, the analysis leading to Eq. (14), together with the assumption of Eq. (20), gives

$$\frac{\left|\frac{dT_e}{dt}\right|}{\left|\frac{dT_i}{dt}\right|} = \frac{\left(\frac{\partial E_i}{\partial T_i}\right)_\rho}{\left(\frac{\partial E_e}{\partial T_e}\right)_\rho} \equiv \frac{C_\rho^i}{C_\rho^e}, \tag{21}$$

the ratio of ionic to electronic specific heats, each evaluated at their respective (e,i) temperatures. For the hydrogen case studied in detail above, we have verified that this prescription produces $C_\rho^i(T_i = 10^5\ \mathrm{K}) \sim C_\rho^e(T_e = 10^7\ \mathrm{K}) \sim \frac{3}{2}k_B/e^-$, and therefore $\frac{C_\rho^i}{C_\rho^e} \approx 1$, when standard EOS models for hydrogen are used [58]. Thus, such an implementation would fail to predict an initial asymmetric T equilibration in this case. The essential missing element is the reduced electron screening (and hence increased effective ion-ion interaction) resulting from $T_e \gg T_i$, which is not captured in a treatment assuming $F_i(\rho,T_i,T_e) = F_i(\rho,T_i)$, for which the screened ion-ion interaction is assumed to be derived from a $T_e = T_i$ or $T_e = 0$ theory. This highlights the importance of improving both the in-line models of the equilibration rate and the EOS model to include more sensible 2T effects at least at the adiabatic level treated, e.g., in our HNC and OF DFT calculations.

C. Energy relaxation versus temperature relaxation

As we mentioned when discussing Fig. 5, the energy relaxation rate (here multiplied by $\frac{2}{3}$ to compare it to temperature relaxation) is quite a bit higher than that as predicted by the Lenard-Balescu theory using the full coupled-mode treatment. In fact, it is rather closer to the predictions of the FGR, in which coupled modes are neglected, in contrast to the conclusions of Ref. [20] for these same plasmas. We now discuss this further.

The definitions we use for the internal energies of electrons and ions, respectively, are those of Eq. (16). Since $E_e + E_i = E_{\mathrm{total}}$, it follows from energy conservation that $dE_i/dt = -dE_e/dt$. It is worth noting that this is true for *any* definition in which V_{ei} is split between electrons and ions, not just the 50%-50% split. As we have seen from the previous discussion, this perfect asymmetry is not enjoyed by dT_i/dt and dT_e/dt, due to the time dependence of the total V. We have picked this particular split of V_{ei} in the internal energies because the authors of Ref. [21] argue that this choice alone makes their general expression for the energy equilibration rate [Eq. (27), and the more approximate Eq. (37) in Ref. [21]] look most like the one derived for weakly coupled plasmas [59] [Eq. (3) in this work or Eq. (7) in Ref. [20]]; if the response functions of the more general expressions are replaced by the RPA response functions, the weakly coupled result is obtained.

The lack of agreement between this expression and the $dE_{e,i}/dt$ from MD for these cases indicates that the response functions at the RPA level are not sufficient. This too was anticipated in the work of Ref. [21], wherein (for hydrogen plasmas with equal densities, but 10 times lower T_i) the inclusion of static ion-ion LFCs derived from HNC was shown to increase the predicted equilibration rate above that of the RPA CM prediction (see black and red curves in Fig. 1 of Ref. [21]). Our analogous predictions appear as the isolated black diamond in Fig. 5; only a very slight increase above the RPA CM LB result (solid black curve and circles) can be seen and the agreement with the energy equilibration rate from MD is therefore still quite poor. Inclusion of all the pairs of static LFCs, G_{ee}, G_{ei}, and G_{ii}, within the dielectric function of Eq. (4) produces almost identical results. We are left to conclude that the standard theories for energy equilibration in 2T plasmas do not apply to at least the semiclassical model of the hydrogen plasmas considered in Ref. [20]. This is troubling for researchers bent on constructing and validating models for energy and temperature equilibration in plasmas with strongly coupled ions [23,24]. In the next section we suggest a possible reason for the inability of the CM Lenard-Balescu theory (with RPA screening and/or with static LFCs) to correctly describe the cases of our study; we propose that a variant of dynamic local-field corrections may be needed here instead. It is worth noting that even in more weakly coupled regimes, our earlier T-equilibration MD vs LB theory comparisons also showed the inclusion of static LFCs to be inadequate (in that case, worse than the RPA result) for oppositely charged two-component plasmas [11].

As shown in Fig. 5, there are two conditions that are approximately satisfied for all the plasmas studied here (if we use the CM LB results, specifically): (i) dT_i/dt (MD) $\approx dT_i/dt$ (LB) $[=\frac{2}{3}dE_{e,i}/dt$ (LB)] and (ii) $-dT_e/dt$ (MD) $\approx \frac{2}{3}dE_{e,i}/dt$ (MD). We currently have no understanding as to why these relations are roughly satisfied; however, it is interesting to note that the simultaneous satisfaction of these conditions puts constraints on the 2T EOS, as expressed in the internal energies of Eq. (16). If we assume that

$$E_e = E_e(T_e, T_i)$$

and

$$E_i = E_i(T_e, T_i)$$

[as in our above assumption, $V = V(T_e, T_i)$], application of the chain rule, together with total energy conservation, produces the equations [21]

$$\begin{aligned} \frac{dE_e}{dt} &\equiv -Z_{\rm MD} = \left(\frac{\partial E_e}{\partial T_e}\right)_{T_i}\frac{dT_e}{dt} + \left(\frac{\partial E_e}{\partial T_i}\right)_{T_e}\frac{dT_i}{dt}, \\ \frac{dE_i}{dt} &\equiv Z_{\rm MD} = \left(\frac{\partial E_i}{\partial T_e}\right)_{T_i}\frac{dT_e}{dt} + \left(\frac{\partial E_i}{\partial T_i}\right)_{T_e}\frac{dT_i}{dt}. \end{aligned} \tag{22}$$

Conditions (i) and (ii) above can be expressed as (a) $dT_{\rm i}/dt$ (MD) $\approx dT_i/dt$ (LB)$= \frac{2}{3}Z_{\rm LB}$ and (b) dT_e/dt (MD)$\approx -\frac{2}{3}dE_i/dt$ (MD)$= -\frac{2}{3}Z_{\rm MD}$. Plugging these conditions into Eqs. (22) and eliminating the ratio $Z_{\rm MD}/Z_{\rm LB}$ yields

$$\left(\frac{\partial E_e}{\partial T_i}\right)_{T_e}\left[\frac{3}{2} + \left(\frac{\partial E_i}{\partial T_e}\right)_{T_i}\right] \approx -\left(\frac{\partial E_i}{\partial T_i}\right)_{T_e}\left[\left(\frac{\partial E_e}{\partial T_e}\right)_{T_i} - \frac{3}{2}\right]. \tag{23}$$

As a concrete example, our HNC estimations, in the manner of Eq. (17), for the $T_i = 10^5$ K and $T_e = 10^7$ K case give for this relation (all numbers expressed in units of k_B)

$$-0.043\left[\tfrac{3}{2} + 0.0011\right] \approx -2.08\left[1.53 - \tfrac{3}{2}\right]$$

or

$$-0.0645 \approx -0.0624,$$

demonstrating once again that our HNC-based theoretical modeling of the nonideal 2T EOS is on solid ground [60]. More fundamentally, the relative magnitudes of the various derivatives in Eqs. (22) and (23) suggest that the much simpler diagonal form of Eq. (22) is quite accurate for these plasmas,

$$\begin{aligned} \frac{dE_e}{dt} &\equiv -Z_{\rm MD} \approx \left(\frac{\partial E_e}{\partial T_e}\right)_{T_i}\frac{dT_e}{dt} \approx \frac{3}{2}\frac{dT_e}{dt}, \\ \frac{dE_i}{dt} &\equiv Z_{\rm MD} \approx \left(\frac{\partial E_i}{\partial T_i}\right)_{T_e}\frac{dT_i}{dt} \approx 2\frac{dT_i}{dt}. \end{aligned} \tag{24}$$

While these observations are clearly borne out in our MD results, we do not claim to understand their origin in a deep sense, beyond the trivial fact that derivatives with respect to T_e are much smaller than derivatives with respect to T_i, due to the small ratio of electronic to ionic coupling. Furthermore, their satisfaction does not explain the surprisingly large $Z_{\rm MD}/Z_{\rm LB}$ that we have found.

The bare ion-ion plasma coupling for the cases studied heretofore is $\Gamma_{ii} \sim 12.5$. While we have argued that this is low enough for an accurate treatment of static correlations within the rubric of HNC, it is possibly too high for a treatment of the equilibration rates using Eq. (3) to be accurate. With this in mind, we also consider the semiclassical hydrogen plasma with $n = 10^{26}$ cm^{-3}, $T_i = 10^6$ K, and $T_e = 10^8$ K. This possesses a bare $\Gamma_{ii} \sim 1.25$, but with a ratio T_e/T_i equal to that of the $T_i = 10^5$ K and $T_e = 10^7$ K case. Table III shows our results. Once again, the energy equilibration rate from MD (expressed as an equivalent temperature derivative: 9.97 eV/fs per k_B) is closer to the FGR rate (10.36 eV/fs) than to the CM LB rate (8.81 eV/fs). Yet again, the two approximate conditions discussed directly above are roughly satisfied. Though the difference between dT_i/dt and $-dT_e/dt$ is far smaller in absolute magnitude due to the smaller ion coupling here, the treatment of Ref. [20] and our Eq. (3) is still sorely incomplete. It remains to be seen if any plasma studied with nonequilibrium classical MD exhibits the coupled-mode effect in the manner predicted by classical Lenard-Balescu theory with RPA screening.

D. Effects of collisional broadening

As discussed in Ref. [20] and in Sec. III of this work, the low-energy, long-wavelength ion-acoustic wave feature in the CM LB treatment is responsible for the marked reduction in equilibration rates relative to the FGR prediction. Furthermore,

TABLE III. Instantaneous dT/dt (in eV/fs) calculated from classical QSP Lenard-Balescu theory and extracted from MD using the identical QSPs for a hydrogen plasma with $n = 10^{26}$ cm^{-3}, $T_i = 10^6$ K, and $T_e = 10^8$ K. Also shown in the rightmost column is the instantaneous rate of change of the internal energy of the ions, expressed as $\frac{2}{3}dE_i/dt$, to compare it to the temperature derivatives (note that the relation $dE_e/dt = -dE_i/dt$ holds exactly, so we only display dE_i/dt).

LB dT_i/dt (no LFCs)	FGR dT_i/dt (no LFCs)	dT_i/dt from MD	$-dT_e/dt$ from MD	$\frac{2}{3}dE_i/dt$ from MD
8.81	10.36	8.73	9.81	9.97

this excitation is predicted to be exceedingly sharp in ω (i.e., long-lived in time), within the standard RPA treatment for the two-component dielectric function that forms the denominator of Eq. (3). It is important to note, however, that MD studies of one- and two-component plasmas in equilibrium have shown that lifetimes of collective modes are greatly reduced relative to those of RPA when the plasma is strongly coupled. For example, the works of Refs. [61–64] demonstrate large deviations of dynamic structure factors $S(k,\omega)$ from their RPA predictions in the neighborhood of plasmon peaks. Specifically, these peaks are substantially broadened and reduced in height when the plasma coupling Γ is of order a few [see, e.g., Figs. 2(c) and 2(d) in Ref. [62]]. Though the static LFCs we have employed in our LB calculations do modify the RPA peak structure in $S(k,\omega)$, they do so primarily by moving the pole positions, rather than by broadening these peaks in frequency. It is therefore of interest to know what effect such a broadening might have on our predictions of T equilibration.

To wit, we employ a simple scheme for affecting such a broadening, that of replacing $\omega \to \omega + i\gamma_i$ in χ_i^0, the density response function of the ions. Here γ_i represents a phenomenological inverse collisional lifetime. Since this replacement in the Lindhard response of Eq. (6) is known to violate local charge conservation, we use instead the modified expression for this function [65], which appears in Refs. [66,67]. This new function $\tilde{\chi}_i^0(k,\omega + i\gamma_i)$ is then input into both the numerator $[\mathrm{Im}\chi_i^0(k,\omega)]$ and the denominator $[D(k,\omega)]$ of Eq. (3), the CM LB expression for dT_i/dt. The electron response function $\chi_e^0(k,\omega)$ is left unchanged in this expression, because the electrons are far more weakly coupled in the cases we consider here ($T_e \gg T_i$ and $\Gamma_{ee} \lesssim 0.125$).

Figure 9 shows a series of $F(k)$ k integrands for the $n = 10^{26}$ cm^{-3}, $T_i = 10^5$ K, and $T_e = 10^7$ K quantum Coulomb hydrogen case, to be compared to those of Fig. 3 above. All have been generated with the aforementioned prescription in which $\tilde{\chi}_i^0(k,\omega + i\gamma_i)$ is used in the context of Eq. (3). Thirteen orders of magnitude in γ_i (in hartree atomic units) are represented. There is a clutch of curves with $10^{-3} < \gamma_i < 10$ located close to the FGR $F(k)$ (black dot-dashed curve) and a collection of curves with $\gamma_i \ll 10^{-3}$ that are essentially indistinguishable from each other and from the RPA CM LB prediction. Figure 10 shows the integrals under these curves $\int_0^\infty dk\, F(k)$ (which are equal to the effective Coulomb logarithm for this case) as a function of γ_i/ω_p, where ω_p is the ion plasma frequency. The y-axis value of

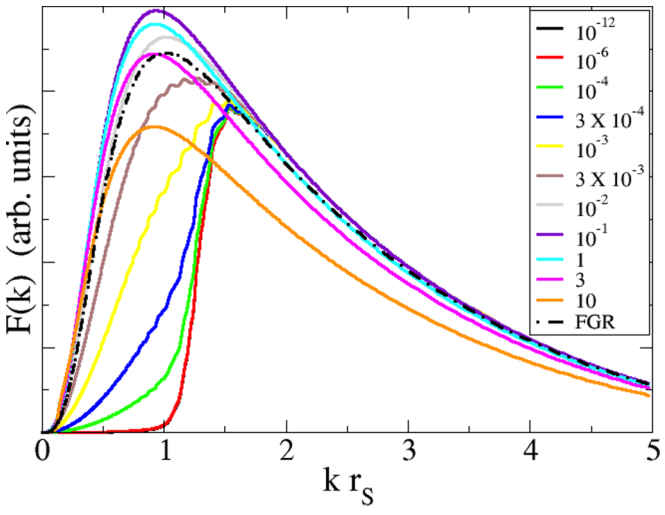

FIG. 9. The k integrands $F(k)$ of Eq. (3) for the quantum Coulomb hydrogen plasma with $n = 10^{26}$ cm^{-3}, $T_i = 10^5$ K, and $T_e = 10^7$ K. Here the Lindhard $\chi_i^0(k,\omega)$ is replaced by the corresponding function $\tilde{\chi}_i^0(k,\omega + i\gamma_i)$ of Refs. [66,67]. Each curve represents a different choice of γ_i, expressed in atomic units (hartrees; see the legend). Note that the $F(k)$ for $\gamma_i = 10^{-12}$ hartree (solid black curve, not shown) and the $F(k)$ for $\gamma_i = 10^{-6}$ hartree (red curve) are essentially identical.

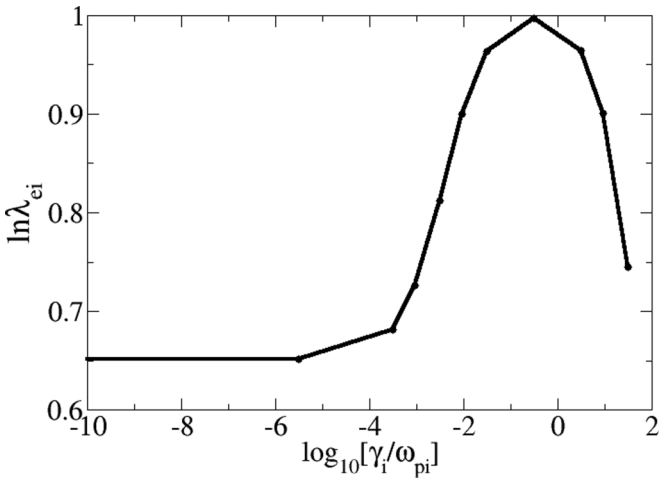

FIG. 10. Effective Coulomb logarithms $\ln\lambda_{ei}$ for the quantum Coulomb hydrogen plasma with $n = 10^{26}$ cm^{-3}, $T_i = 10^5$ K, and $T_e = 10^7$ K. Here the Lindhard $\chi_i^0(k,\omega)$ in Eq. (3) is replaced by the corresponding function $\tilde{\chi}_i^0(k,\omega + i\gamma_i)$ of Refs. [66,67]. Each point on the curve represents a different choice of γ_i. The CM LB RPA result is represented by the nearly flat line on the bottom left of the plot; the FGR result is at $\ln\lambda_{ei} \sim 0.95$.

$\sim$0.65 denotes the effective $\ln\lambda_{ei}$ corresponding to the CM LB prediction, while the FGR value is in the neighborhood of $\ln\lambda_{ei} = 0.95$. Thus, it appears that the phenomenological collisional broadening applied solely to the strongly coupled ions can indeed extinguish the CM effect, if the collision frequency is in the appropriate range.

As an independent estimate of this ion collision frequency, we turn to MD simulations of ion OCPs with plasma conditions similar to ours in this case ($\Gamma \sim 12.5$). The work of Ref. [61] displays MD data for $S(k,\omega)$ for a plasma with $\Gamma = 9.7$ (see Fig. 5 therein). We are concerned primarily with k values of the order of $\sim 1/r_S$, given our discussion surrounding our Fig. 3. Both $k = 0.6187/r_S$ and $k = 1.3837/r_S$ were considered in Ref. [61]. To affect a comparison, we evaluate $\tilde{\chi}_i^0(k,\omega + i\gamma_i)$ for the $\Gamma = 9.7$ OCP at these specific k and for a range of γ_i. From these, we compute the interacting $\tilde{\chi}_i$ functions (which would correspond to the RPA χ in the limit of $\gamma_i \to 0$), using the usual relation

$$\tilde{\chi}_i(k,\omega) = \frac{\tilde{\chi}_i^0(k,\omega)}{1 - v(k)\tilde{\chi}_i^0(k,\omega)}. \tag{25}$$

The dynamic structure factors are then computed from these polarizabilities using the fluctuation-dissipation theorem [39]. Good agreement with the MD results of Ref. [61] are found when γ_i is chosen to be roughly $0.1\omega_p$–$0.2\omega_p$. The plot of Fig. 10 shows this to be in the range where the FGR result is expected. Yet another estimate for γ_i can be obtained by appealing to the relationship between this quantity and the self-diffusion constant D outlined in Ref. [68] (see Chap. 9 therein) and alluded to in Ref. [69]:

$$\gamma = \frac{k_B T}{mD}, \tag{26}$$

where m is the ion mass. Using the diffusion constant for the $\Gamma = 9.7$ plasma quoted in Table II of Ref. [61], we obtain $\gamma_i = 0.26\omega_p$, once again in the range clearly favoring the FGR result. Finally, our own MD computation of $S(k = 0.3/r_S,\omega)$ for the $\Gamma = 12.5$ OCP shows a plasmon peak with a full width at half maximum of $\sim 0.1\omega_p$, again indicating a γ_i in this same range.

We therefore deem it highly likely that collisional broadening among the strongly coupled ions is responsible for extinguishing the coupled-mode effect. It may prove fruitful in future studies to explore more complex k-dependent models for γ_i [63,64] as well as more sophisticated (beyond-RPA) treatments of the plasma dispersion relation to refine these predictions of $S_{ii}(k,\omega)$ further, as they apply to the equilibration problem. More fundamentally, however, it is unknown at present if the GLB prescription, as exhibited in Eq. (3), is truly up to the task of handling such problems; our lifetime-broadened $S_{ii}(k,\omega)$ is essentially equivalent to some specific dynamical local-field correction $[G_{ii}(k,\omega)]$ as appearing in Eqs. (3) and (4), but for sufficiently strong plasma couplings, even this picture is likely to be inadequate for readily accessible $G(k,\omega)$.

E. Effect of non-Maxwellian velocity distributions

Because the plasmas we consider here have such large initial T splits and the cases we have studied exhibit distinct

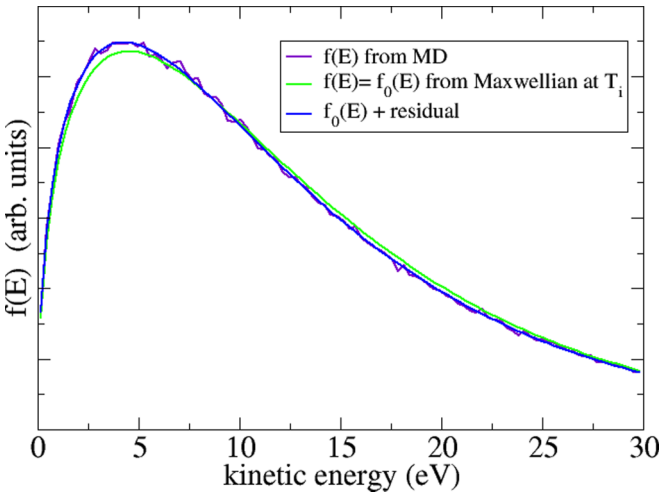

FIG. 11. Ion kinetic energy distributions from MD (purple), together with the closest-fit Maxwellian distribution.

kinetic and configurational ion temperatures, it is of interest to know if the assumption of Maxwellian velocity distributions (which we have made thus far in the theoretical estimates) is truly well founded for the time intervals over which MD data has been taken. It is conceivable that the disagreements we have seen, LB theory vs MD, result in part from the inadequacy of the Maxwellian assumption. To this end, we examine the velocity distributions from MD, $f_e(v)$ and $f_i(v)$, at representative times for the trajectory corresponding to the $n = 10^{26}$ cm^{-3}, $T_i = 10^5$ K, and $T_e = 10^7$ K case. Figure 11 shows the ion distribution (purple) from our MD simulation, together with the Maxwellian distribution (green) at the T_i corresponding to the total ion kinetic energy at this t. A small but systematic deviation between the two is noticeable. Figure 12 shows the residual (purple curve minus green curve in Fig. 11) over this same energy range (purple).

The green curve in Fig. 12 is our smooth fit to this residual, constructed by expanding the multiplicative deviation of $f_i(v)$ from the Maxwellian distribution $f_i^{(0)}(v)$ in a series of Laguerre polynomials

$$f_i(v) = f_i^{(0)}(v)\sum_{n=0}^{\infty} A_n^i L_n^{(1/2)}\left(\frac{m_i\beta_i v^2}{2}\right). \tag{27}$$

We find that the residual is best fit with just the first nonunity term in this expansion. The blue curve in Fig. 11 shows $f_i^{(0)}(v)$ plus our fit to the residual. The electron distribution at this same time (and for all times) has practically no residual at all; this is to be expected from the fact that the ions move much more slowly than the electrons and are therefore slower to come into intraspecies equilibrium [70].

Using the mathematical techniques employed in Ref. [71], we predict that the ion residual shown in Fig. 12 increases the LB prediction of dT_i/dt by only $\sim$3%, relative to that of the perfect Maxwellian distribution with $T = T_i$. Details of this calculation are given in the Appendix. This then demonstrates that intraspecies equilibration is indeed much faster than the time scale for interspecies heat exchange of primary interest in this work, as expected. Thus, despite the large initial T splits that could in principle have skewed the MD velocity

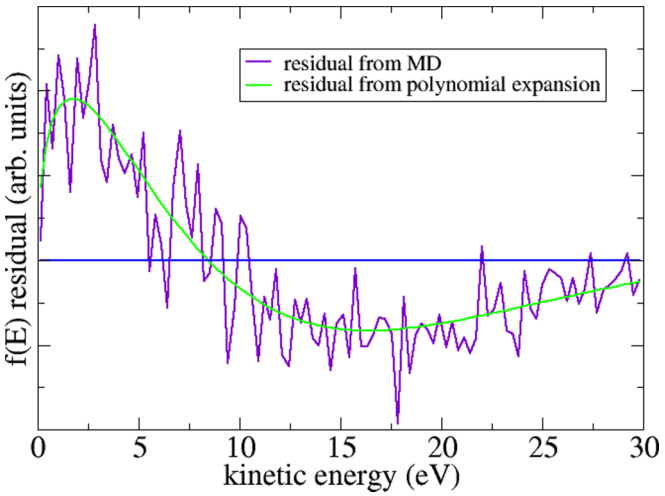

FIG. 12. The $\mathcal{E}_i$-dependent residual, together with a fit comprised (chiefly) of a single Laguerre polynomial.

distributions appreciably at later times, we conclude that the plasmas we study here are indeed amenable to theoretical T-equilibration treatments that assume Maxwellian velocity distributions. However, the failure of the ion static structure [represented by $g_{ii}(r)$] to reflect the correlations of a system of ions in thermal equilibrium at the kinetic temperature T_i is another matter entirely and is undoubtedly a manifestation of nonadiabatic effects that are beyond the scope of our current theoretical tools [in the manner of Eq. (3)].

V. CONCLUSION

We have presented nonequilibrium classical molecular dynamics results for temperature equilibration of hydrogen plasmas at a density of $n = 10^{26}$ cm^{-3}. Interparticle interactions were taken to be QSPs of the Dunn-Broyles [27] and Minoo *et al.* [28] forms [35]. The initial temperatures considered, $T_i = 10^5$ K and T_e between 10^7 and 5×10^8 K, were chosen to coincide with those studied in a paper of Vorberger and Gericke [20] in which they used the Lenard-Balescu equation to predict that the energy equilibration rate for such systems is substantially lowered due to the presence of ion acoustic waves. Our Lenard-Balescu calculations for the associated classical QSP plasmas also predict a corresponding reduction, but fail to agree with the energy equilibration rates from our MD. Inclusion of static local-field corrections in the (generalized) Lenard-Balescu calculations does little to improve this. However, replacing the Lindhard ion density response function χ_i^0 by one in which collisional broadening is assumed largely extinguishes the coupled-mode effect.

The large differences between T_e and T_i complicate the preparation of nonequilibrium systems compared to what has been studied the past [11,13]. Thus, we discussed the relative merits of three schemes for initializing the MD simulations. The evaluation of the Lenard-Balescu equilibration rate is also more complex when the plasmas considered are in this regime; our strategy for computing it was described and comparisons were made to the analogous strategies and results outlined in Ref. [20].

We found that for the cases we studied with MD, there is a sizable effect on dT_e/dt and dT_i/dt from time-varying potential energy, not treated in the usual Lenard-Balescu approach, but discussed in detail in various recent works [7,14,21]. We used a variety of approaches to quantify this effect and we also demonstrated that it should be present for real quantum hydrogen plasmas in these conditions as well (i.e., not just for the classical QSP model of hydrogen with which we have conducted our MD simulations of T equilibration). In addition, we observed that the static structure of the ions in our classical MD simulations is notably different (more structured) from that corresponding to ions in thermal equilibrium at the instantaneous kinetic T_i. This may very well result from strong nonadiabatic effects in the systems under consideration, the implications of which must be studied further.

Our MD results and associated comparisons to theory constitute a crucial step in validating and critiquing new models for temperature equilibration [23,24] aimed at treating plasmas for which the electron-electron and electron-ion couplings may be weak, but the ion-ion coupling is somewhat stronger. In addition to being of potential interest to the field of laser-produced plasmas (where, generally, $T_e \gg T_i$ initially), this sets the stage for the investigation of plasmas containing multiple ion species where some of these ions have a sizable average charge. Such cases have also been predicted to be strongly affected by coupled collective modes [see Eq. (1)]. However, we are now faced with the troubling result that the coupled-mode effect itself seems to be greatly exaggerated in the available theories, at least for the two-species plasmas we have considered in this work. It is entirely possible that the ion acoustic waves that constitute the coupled modes here are so severely underdamped as to be veritably decoupled from the other modes (e.g., plasmons) in the system; in this case, such modes may not thermalize sufficiently to steal oscillator strength away from the plasmons, as they are assumed to do in the coupled-mode Lenard-Balescu treatment [20]. Still another potential explanation is that stemming from the calculations we have outlined in Sec. IV D, collisional broadening within the strongly coupled ion subsystem.

It remains to be seen if a more sophisticated treatment of the coupled electron-ion density response [21] yields more favorable comparisons with MD or if the linear response assumption itself is questionable in these $T_e \gg T_i$ cases.

ACKNOWLEDGMENTS

We thank D. O. Gericke, J. Vorberger, D. A. Chapman, H. D. Whitley, and A. Pribram-Jones for helpful discussions. This work was performed under the auspices of the US Department of Energy by Lawrence Livermore National Laboratory under Contract No. DE-AC52-07NA27344 and by Los Alamos National Laboratory under Contract No. DE-AC52-06NA25396.

APPENDIX A: MODEL FOR THE INTERNAL ENERGY OF A 2T HYDROGEN PLASMA

To approximate the internal energy of a real Coulomb system, we follow a derivation similar to that given by Ashcroft and Stroud [45]. The general Hamiltonian of a Coulomb

system (classical or quantum) can be written as

$$\begin{aligned}\mathscr{H} = &\sum_i \frac{p_i^2}{2m} + \frac{1}{2}\sum_{i\neq i'} \frac{e^2}{|\mathbf{r}_i - \mathbf{r}_{i'}|} - E_0 \\ &+ \frac{1}{2}\sum_{j\neq j'} \frac{Z^2e^2}{|\mathbf{R}_j - \mathbf{R}_{j'}|} + E_1 + E_0 \\ &- \sum_{i,j} \frac{Ze^2}{|\mathbf{r}_i - \mathbf{R}_j|} - E_1 + \sum_j \frac{P_j^2}{2M},\end{aligned} \tag{A1}$$

where n_e is the mean electron number density, E_0 is the self-energy of a uniform background of charge density $n_e e$ given by

$$E_0 = \frac{1}{2}\int d\mathbf{r}\int d\mathbf{r}' \frac{(n_e e)^2}{|\mathbf{r}-\mathbf{r}'|}, \tag{A2}$$

and E_1 is the interaction between the ions and this background

$$E_1 = \frac{1}{2}\sum_j \int d\mathbf{r} \frac{Ze^2 n_e}{|\mathbf{r}-\mathbf{R}_j|}. \tag{A3}$$

Here $\{\mathbf{r}_i\}$ and $\{\mathbf{R}_j\}$ denote electronic and ionic coordinates, respectively, with $\{\mathbf{p}_i\}$ and $\{\mathbf{P}_j\}$ being their momenta and m and M being their masses. Lines 1–3 of (A1) have been arranged to yield components that are individually finite in the thermodynamic limit. For example, line 1 of (A1) is simply the Hamiltonian of a free electron gas $\mathscr{H}_{\rm FEG}$ embedded in a neutralizing uniform background. The rest of (A1), minus the last term, can be expressed in Fourier space as

$$\mathscr{V}_{ii} = \frac{Z^2}{2}\int \frac{d\mathbf{k}}{(2\pi)^3} v_{ee}(k)[\hat{n}_{\rm ion}(\mathbf{k})\hat{n}_{\rm ion}(-\mathbf{k}) - N_{\rm ion}], \tag{A4}$$

$$\mathscr{V}_{ei} = -\frac{Z}{2}\int \frac{d\mathbf{k}}{(2\pi)^3} v_{ee}(k)\hat{n}_{\rm ion}(\mathbf{k})\hat{n}_e(-\mathbf{k}), \tag{A5}$$

where $\hat{n}_{\rm ion}(\mathbf{k})$ and $\hat{n}_e(\mathbf{k})$ are the ion and electron density operators respectively, $N_{\rm ion}$ is the total number of ions, and $v_{ee}(k) = 4\pi e^2/k^2$.

Generally speaking, the statistical mechanics of a two-temperature system is poorly defined [44]. However, for the electron-proton system of interest, we can simplify the calculations by approximating the ions as classical point particles and temporarily fixing their coordinates, which is reasonable given their mass discrepancy ($M/m \approx 1836$) and lower temperature ($T_i/T_e \leqslant 1/100$). The ensemble average over the electron degrees of freedom in terms of T_e generates the internal energy of the electron gas $\langle\mathscr{H}_{\rm FEG}\rangle = N_{\rm ion}U_{\rm FEG}(n_e,T_e)$ and the electron density $\langle\hat{n}_{\rm e}(\mathbf{k})\rangle$ and leaves the remaining variables unchanged. This procedure is equivalent to the Born-Oppenheimer approximation.

We next approximate the electron density in terms of the ion density operator through a response function as

$$\langle\hat{n}_e(\mathbf{k})\rangle \approx -Zv_{ee}(k)\chi(k;n_e,T_e)n_{\rm ion}(\mathbf{k}). \tag{A6}$$

In general, this response function would be calculated in terms of cross correlations between the ions and electrons and thus depend on both temperatures; however, the response will be dominated by the electron temperature for the problem of interest due to the previously mentioned disparate quantities [46,48]. Next the ionic coordinates are released and an ensemble average is taken in terms of the ionic degrees of freedom and T_i. Using the definition of the ion-ion static structure factor

$$S_{ij}(k) \equiv \frac{1}{\sqrt{N_i N_j}}\langle\hat{n}_i(\mathbf{k})\hat{n}_j(-\mathbf{k})\rangle, \tag{A7}$$

we obtain the expression for the total internal energy

$$\begin{aligned}\langle\mathscr{H}\rangle &= N_{\rm ion}U_{\rm int} \\ &= N_{\rm ion}U_{\rm FEG}(n_e,T_e) \\ &\quad + N_{\rm ion}\frac{Z^2}{2}\int\frac{d\mathbf{k}}{(2\pi)^3}v_{ee}(k)[S_{ii}(k)-1] \\ &\quad + N_{\rm ion}\frac{Z^2}{2}\int\frac{d\mathbf{k}}{(2\pi)^3}v_{ee}^2(k)\chi(k)S_{ii}(k) + \frac{3}{2}N_{\rm ion}k_BT_i,\end{aligned} \tag{A8}$$

where lines 2–4 of (A8) correspond to lines 1–3 of (A1), respectively. By next introducing the dielectric function $\epsilon^{-1}(k) = 1 + v_{ee}(k)\chi(k)$, we can write the internal energy per ion as

$$U_{\rm int} = U_{\rm FEG} + \tfrac{3}{2}k_BT_i + \tfrac{Z^2}{2}\int\tfrac{d\mathbf{k}}{(2\pi)^3}v_{ee}(k)\left[\tfrac{S_{ii}(k)}{\epsilon(k)} - 1\right]. \tag{A9}$$

As a simple model, we take the response function associated with the linearized Thomas-Fermi (TF) functional. Within this approximation, the dielectric function takes the form $\epsilon(k) \approx 1 + (\lambda_{\rm TF}k)^{-2}$, where the TF screening length is $\lambda_{\rm TF}^{-2} = 4\pi e^2(\partial n_e/\partial\mu)$, with

$$n_e = 2\int\frac{d\mathbf{p}}{(2\pi)^3}(1 + e^{(p^2/2m-\mu)/T_e})^{-1}. \tag{A10}$$

More complicated energy functionals have been explored with gradient corrections to the density and exchange-correlation effects, but these higher-order contributions were found to be negligible for the system of interest [72]. The resulting internal energy then simplifies to

$$\begin{aligned}U_{\rm int} = U_{\rm FEG}(n_e,T_e) &+ \frac{3}{2}k_BT_i - \frac{Z^2}{2\lambda_{\rm TF}} \\ &+ 2\pi Z^2 n_{\rm ion}\int_0^\infty dr\, e^{-r/\lambda_{\rm TF}}r[g_{ii}(r)-1],\end{aligned} \tag{A11}$$

where $g_{ii}(r)$ is the ion-ion radial distribution function. Finally, the internal energy of the electron gas can be estimated using fits from Ref. [51], while the final potential energy term in Eq. (A11) can calculated using the HNC approximation with the appropriate screened Coulomb (Yukawa) interaction.

APPENDIX B: EQUILIBRATION RATES FOR NON-MAXWELLIAN DISTRIBUTIONS

We compute energy equilibration for a plasma with electrons and one ion species, for the case of general particle distributions that include small non-Maxwellian components, using the quantum Lenard-Balescu equation. Though our primary aim in the bulk of the main text is the analysis of classical plasmas, we use the quantum LB equation here because the quantum LB collision operator is mathematically more straightforward to handle in this context. However, we expect

the effects of non-Maxwellian distributions on equilibration rates to be largely insensitive to this distinction. Considering two species, electrons and protons, their distributions are written as

$$f_e(v) = f_e^{(0)}(\mathbf{v}) \sum_{n=0}^{\infty} A_n^e L_n^{(1/2)}\left(\frac{m_e \beta_e v^2}{2}\right), \tag{B1}$$

$$f_i(v) = f_i^{(0)}(\mathbf{v}) \sum_{n=0}^{\infty} A_n^i L_n^{(1/2)}\left(\frac{m_i \beta_i v^2}{2}\right), \tag{B2}$$

where $f_e^{(0)}$ and $f_i^{(0)}$ are Maxwellian distributions and $L_n^{(1/2)}$ are Laguerre polynomials, which allow for complete flexibility in the shapes of the distributions. Conservation of the number of particles for each species requires [71]

$$A_0^e = A_0^i = 1. \tag{B3}$$

The condition for kinetic energy conservation (this is all we can assume here, given our use of the LB equation [16]) can be derived from

$$\mathcal{E}_e = \frac{3}{2}\frac{n_e}{\beta_e}, \quad \mathcal{E}_i = \frac{3}{2}\frac{n_i}{\beta_i}, \tag{B4}$$

which gives

$$A_1^e = A_1^i = 0. \tag{B5}$$

Since, for hydrogen, we have $n_e = n_i$,

$$\beta_i A_1^e = -\beta_e A_1^i. \tag{B6}$$

The two-species LB kinetic equation is of the form

$$\frac{\partial f_e}{\partial t} = C_{ee}(f_e) + C_{ei}(f_e, f_i), \tag{B7}$$

$$\frac{\partial f_i}{\partial t} = C_{ii}(f_i) + C_{ie}(f_e, f_i). \tag{B8}$$

The intraspecies collision operators C_{ee} and C_{ii} are irrelevant for energy equilibration. We compute the time rate of change of the ion energy

$$\frac{d(\mathcal{E})_i}{dt} = \frac{1}{2} m_i \int v^2 C_{ie}(f_e, f_i) d^3\mathbf{v}. \tag{B9}$$

The collision operator is given by [73]

$$C_{ie}(f_e, f_i) = -\frac{1}{4\pi^2\hbar^2}\int d^3\mathbf{v}' \int d^3\mathbf{k} \frac{|\phi_{ei}(k)|^2}{\left|\epsilon\left(k, \mathbf{k}\cdot\mathbf{v} + \frac{\hbar k^2}{2m_i}\right)\right|^2} \times \delta[\mathbf{k}\cdot(\mathbf{v}-\mathbf{v}') + \hbar k^2/2\mu] \times [f_i(\mathbf{v}) f_e(\mathbf{v}') - f_i(\mathbf{v}+\hbar\mathbf{k}/m_i) f_e(\mathbf{v}' - \hbar\mathbf{k}/m_e)], \tag{B10}$$

where

$$\mu \equiv \frac{m_e m_i}{m_e + m_i} \tag{B11}$$

is the reduced mass. Next we plug the distributions (B1) and (B2) into (B9) and use various identities to perform the integrals. The $\mathbf{v}'$ integrals can be handled immediately,

$$I_1(k,\omega) \equiv \int d^3\mathbf{v}' \delta(\omega_+ - \mathbf{k}\cdot\mathbf{v}') f_e(\mathbf{v}') = n_e \left(\frac{\beta_e m_e}{2\pi}\right)^{1/2} \frac{1}{k} \sum_n A_n^e L_n^{(-1/2)}(Y_+^2) e^{-Y_+^2}, \tag{B12}$$

$$I_2(k,\omega) \equiv \int d^3\mathbf{v}' \delta(\omega_+ - \mathbf{k}\cdot\mathbf{v}') f_e(\mathbf{v}' - \hbar\mathbf{k}/m_e) = n_e \left(\frac{\beta_e m_e}{2\pi}\right)^{1/2} \frac{1}{k} \sum_n A_n^e L_n^{(-1/2)}(Y_-^2) e^{-Y_-^2}, \tag{B13}$$

where

$$\omega \equiv \mathbf{k}\cdot\mathbf{v} + \frac{\hbar k^2}{2m_i}, \tag{B14}$$

$$\omega_\pm \equiv \omega \pm \frac{\hbar k^2}{2m_e}, \tag{B15}$$

and

$$Y_\pm^2 \equiv \frac{m_e \beta_e \omega_\pm^2}{2k^2}. \tag{B16}$$

We then have

$$\frac{d(\mathcal{E})_i}{dt} = -\frac{1}{4\pi^2\hbar^2}\frac{1}{2} m_i \int d^3\mathbf{v} \int d^3\mathbf{k} \frac{|\phi_{ei}(k)|^2}{|\epsilon(k,\omega)|^2} v^2 \times [f_i(\mathbf{v}) I_1(k,\omega) - f_i(\mathbf{v}+\hbar\mathbf{k}/m_i) I_2(k,\omega)]. \tag{B17}$$

Turning to the $\mathbf{v}$ integrals,

$$J_1(k) \equiv \int d^3\mathbf{v} \frac{|\phi(k)|^2}{|\epsilon(k,\omega)|^2} v^2 f_i(\mathbf{v}) I_1(k,\omega), \tag{B18}$$

$$J_2(k) \equiv \int d^3\mathbf{v} \frac{|\phi(k)|^2}{|\epsilon(k,\omega)|^2} v^2 f_i(\mathbf{v}+\hbar\mathbf{k}/m_p) I_2(k,\omega). \tag{B19}$$

For these, we assume the $\mathbf{k}$ vector points in the z direction so that

$$v_z = \frac{\overline{\omega}_-}{k}, \tag{B20}$$

$$dv_z = \frac{1}{k} d\omega, \tag{B21}$$

and

$$v^2 = v_\perp^2 + \left(\frac{\overline{\omega}_-}{k}\right)^2, \tag{B22}$$

where

$$\overline{\omega}_\pm \equiv \omega \pm \frac{\hbar k^2}{2m_i}. \tag{B23}$$

To evaluate $J_1(k)$ and $J_2(k)$, we need the identities

$$\int_0^\infty e^{-\beta_i m_i v_\perp^2/2} L_m^{(1/2)}\left(\frac{\beta_i m_i v_\perp^2}{2} + \frac{\beta_i m_i v_z^2}{2}\right) v_\perp dv_\perp = \frac{1}{\beta_i m_i} L_m^{(-1/2)}\left(\frac{\beta_i m_i v_z^2}{2}\right) \tag{B24}$$

and

$$\int_0^\infty e^{-\beta_i m_i v_\perp^2/2} L_m^{(1/2)}\left(\frac{\beta_i m_i v_\perp^2}{2}+\frac{\beta_i m v_z^2}{2}\right) v_\perp^3 dv_\perp = \frac{4}{(\beta_i m_i)^2} L_m^{(-3/2)}\left(\frac{\beta_i m_i v_z^2}{2}\right). \tag{B25}$$

Note that

$$\frac{\beta_i m_i v_z^2}{2} = \overline{Y}_-^2, \tag{B26}$$

where

$$\overline{Y}_-^2 \equiv \frac{\beta_i m_i \overline{\omega}_\pm^2}{2k^2}\,. \tag{B27}$$

Using these relations, we obtain

$$J_1(k) = \sqrt{\frac{2}{\pi}}\frac{n_i}{\sqrt{m_i\beta_i}}\sum_m A_m^i \int_{-\infty}^\infty \frac{|\phi(k)|^2}{|\epsilon(k,\omega)|^2} e^{-\overline{Y}_-^2} \times \left[2L_m^{(-3/2)}(\overline{Y}_-^2) + \overline{Y}_-^2 L_m^{(-1/2)}(\overline{Y}_-^2)\right]\frac{I_1(k,\omega)}{k} d\omega. \tag{B28}$$

To compute $J_2(k)$, we make the substitution $\mathbf{u} = \mathbf{v} + \hbar\mathbf{k}/m_p$. Because we choose $\mathbf{k}$ to point in the z direction, we have

$$v^2 = u_\perp^2 + \left(\frac{\overline{\omega}_-}{k}\right)^2 \tag{B29}$$

and we can immediately write

$$J_2(k) = \sqrt{\frac{2}{\pi}}\frac{n_i}{\sqrt{m_i\beta_i}}\sum_m A_m^i \int_{-\infty}^\infty \frac{|\phi(k)|^2}{|\epsilon(k,\omega)|^2} e^{-\overline{Y}_+^2} \times \left[2L_m^{(-3/2)}(\overline{Y}_+^2) + \overline{Y}_-^2 L_m^{(-1/2)}(\overline{Y}_+^2)\right]\frac{I_2(k,\omega)}{k} d\omega. \tag{B30}$$

The equilibration rate is given by

$$\frac{d(\mathcal{E})_i}{dt} = -\frac{m_i}{2\pi\hbar^2}\int_0^\infty [J_1(k) - J_2(k)]k^2 dk. \tag{B31}$$

Noting that $I_1(k,\omega) = I_2(k,-\omega)$, we can show by the substitution $\omega \to -\omega$ that

$$J_2(k) = \sqrt{\frac{2}{\pi}}\frac{n_i}{\sqrt{m_i\beta_i}}\sum_m A_m^i \int_{-\infty}^\infty \frac{|\phi(k)|^2}{|\epsilon(k,\omega)|^2} e^{-\overline{Y}_-^2} \times \left[2L_m^{(-3/2)}(\overline{Y}_-^2) + \overline{Y}_+^2 L_m^{(-1/2)}(\overline{Y}_-^2)\right]\frac{I_1(k,\omega)}{k} d\omega \tag{B32}$$

and

$$J_1(k) - J_2(k) = \sqrt{\frac{2}{\pi}}\frac{n_i}{\sqrt{m_i\beta_i}}\sum_m A_m^i \int_{-\infty}^\infty \frac{|\phi(k)|^2}{|\epsilon(k,\omega)|^2} e^{-\overline{Y}_-^2} \times \left[(\overline{Y}_-^2 - \overline{Y}_+^2)L_m^{(-1/2)}(\overline{Y}_-^2)\right]\frac{I_1(k,\omega)}{k} d\omega. \tag{B33}$$

We now need to plug $I_1(k,\omega)$ into this formula, which we do by making use of the identities

$$\overline{Y}_-^2 - \overline{Y}_+^2 = -\beta_i\hbar\omega \tag{B34}$$

and

$$\overline{Y}_-^2 + Y_+^2 = \frac{m_i\beta_i}{2k^2}(1+\alpha)\omega^2 + \frac{\hbar\omega}{2}(\beta_e - \beta_i) + \frac{\hbar^2k^2}{8}\left(\frac{\beta_i}{m_i} + \frac{\beta_e}{m_e}\right), \tag{B35}$$

where

$$\alpha \equiv \frac{m_e\beta_e}{m_i\beta_i}. \tag{B36}$$

Putting these pieces together, we find

$$\frac{d(\mathcal{E})_i}{dt} = 8n_e n_i\sqrt{\frac{\beta_e}{2m_i}}e^4 \sum_{m=0}^\infty\sum_{n=0}^\infty A_n^e A_m^i \times \int_0^\infty\int_{-\infty}^\infty \frac{e^{-(1+\alpha)x^2}}{|\epsilon(x,y)|^2}\frac{e^{-\sqrt{m_e/m_i}2xy(\gamma-1)}}{y^2} e^{-(\gamma+m_e/m_i)y^2} \times L_m^{(-1/2)}(\overline{Y}_-^2)L_n^{(-1/2)}(Y_+^2)x\,dx\,dy, \tag{B37}$$

where we have used the dimensionless variables

$$x^2 = \frac{m_i\beta_i\omega^2}{2k^2}, \quad y^2 \equiv \frac{\hbar^2\beta_i k^2}{8m_e}, \quad \gamma \equiv \frac{\beta_e}{\beta_i} = \frac{T_i}{T_e}, \tag{B38}$$

which lead to

$$Y_\pm = \sqrt{\alpha}x \pm \sqrt{\gamma}y, \tag{B39}$$

$$\overline{Y}_\pm = x \pm \sqrt{\frac{m_e}{m_i}}y. \tag{B40}$$

Now we need the two-component RPA dielectric function for which the distributions of (B1) and (B2) are used. This is derived in Appendix A of Ref. [71] (see also [74]):

$$\epsilon(x,y) = 1 + \frac{\eta^2}{y^2}\left[w^i(x) + \frac{\xi\gamma}{Z^2}w^e(x)\right], \tag{B41}$$

where

$$w_r^i(x) = \sum_k A_k^i M\left(k+1,\frac{1}{2};-x^2\right), \tag{B42}$$

$$w_i^i(x) = \sqrt{\pi}xe^{-x^2}\sum_k A_k^i L_k^{(-1/2)}(x^2) \tag{B43}$$

and

$$w_r^e(x) = \sum_k A_k^e M\left(k+1,\frac{1}{2};-\alpha x^2\right), \tag{B44}$$

$$w_i^e(x) = \sqrt{\pi}\sqrt{\alpha}xe^{-\alpha x^2}\sum_k A_k^e L_k^{(-1/2)}(\alpha x^2). \tag{B45}$$

Here $M(a,b;z)$ is the confluent hypergeometric function. This result, together with (B37) and the method of Appendix C of Ref. [71], provides us with the means to compute (kinetic) energy equilibration rates for non-Maxwellian particle distributions within the LB theory.

[1] E. I. Moses, R. N. Boyd, B. A. Remington, C. J. Keane, and R. Al-Ayat, Phys. Plasmas **16**, 041006 (2009).

[2] S. Azteni and J. Meyer-ter-Vehn, *The Physics of Inertial Fusion* (Clarendon, Oxford, 2004).

[3] G. Faussurier and C. Blancard, Phys. Rev. E **93**, 023204 (2016).

[4] M. W. C. Dharma-wardana and F. Perrot, Phys. Rev. E **58**, 3705 (1998).

[5] L. S. Brown, D. L. Preston, and R. L. Singleton, Jr., Phys. Rep. **410**, 237 (2005).

[6] D. O. Gericke, M. S. Murillo, and M. Schlanges, Phys. Rev. E **65**, 036418 (2002).

[7] D. O. Gericke, J. Phys.: Conf. Ser. **11**, 111 (2005).

[8] J. Daligault and G. Dimonte, Phys. Rev. E **79**, 056403 (2009).

[9] G. Dimonte and J. Daligault, Phys. Rev. Lett. **101**, 135001 (2008).

[10] J. P. Hansen and I. R. McDonald, Phys. Lett. **97A**, 42 (1983).

[11] L. X. Benedict, M. P. Surh, J. I. Castor, S. A. Khairallah, H. D. Whitley, D. F. Richards, J. N. Glosli, M. S. Murillo, C. R. Scullard, P. E. Grabowski, D. Michta, and F. R. Graziani, Phys. Rev. E **86**, 046406 (2012).

[12] B. Jeon, M. Foster, J. Colgan, G. Csanak, J. D. Kress, L. A. Collins, and N. Gronbech-Jensen, Phys. Rev. E **78**, 036403 (2008).

[13] J. N. Glosli, F. R. Graziani, R. M. More, M. S. Murillo, F. H. Streitz, M. P. Surh, L. X. Benedict, S. Hau-Riege, A. B. Langdon, and R. A. London, Phys. Rev. E **78**, 025401(R) (2008).

[14] L. X. Benedict, J. N. Glosli, D. F. Richards, F. H. Streitz, S. P. Hau-Riege, R. A. London, F. R. Graziani, M. S. Murillo, and J. F. Benage, Phys. Rev. Lett. **102**, 205004 (2009).

[15] L. D. Landau, Phys. Z. Sowjetuniuon **10**, 154 (1936); Zh. Eksp. Teor. Fiz. **7**, 203 (1937); L. Spitzer, Jr., *Physics of Fully Ionized Gases*, 2nd ed. (Interscience, New York, 1962).

[16] R. Balescu, *Statistical Mechanics of Charged Particles* (Wiley Interscience, New York, 1963).

[17] M. W. C. Dharma-wardana also worked on this topic several years earlier, in the context of solids. See, e.g., M. W. C. Dharma-wardana, Solid State Commun. **86**, 83 (1993).

[18] P. Celliers, A. Ng, G. Xu, and A. Forsman, Phys. Rev. Lett. **68**, 2305 (1992); A. Ng, P. Celliers, G. Xu, and A. Forsman, Phys. Rev. E **52**, 4299 (1995).

[19] G. Gregori and D. O. Gericke, Europhys. Lett. **83**, 15002 (2008).

[20] J. Vorberger and D. O. Gericke, Phys. Plasmas **16**, 082702 (2009).

[21] J. Vorberger, D. O. Gericke, T. Bornath, and M. Schlanges, Phys. Rev. E **81**, 046404 (2010).

[22] The derivation of this inequality appears in Appendix C of Ref. [20] and arises from the fact that an ion acoustic mode exists when the negative ion susceptibility exceeds the positive electron susceptibility, which in turn results when the electron screening length is greater than $1/\sqrt{0.27}$ times the ion screening length. This condition expands upon the more approximate relation $T_i \ll T_e$, which is discussed, e.g., by E. M. Lifshitz and L. P. Pitaevskii, *Physical Kinetics* (Pergamon, New York, 1981), Sec. 33.

[23] D. A. Chapman, J. Vorberger, and D. O. Gericke, Phys. Rev. E **88**, 013102 (2013).

[24] W. J. Garbett and D. A. Chapman, J. Phys.: Conf. Ser. **688**, 012019 (2016).

[25] M. S. Murillo and M. W. C. Dharma-wardana, Phys. Rev. Lett. **100**, 205005 (2008).

[26] J. Vorberger and D. O. Gericke, High Energy Density Phys. **10**, 1 (2014).

[27] T. Dunn and A. A. Broyles, Phys. Rev. **157**, 156 (1967).

[28] H. Minoo, M. M. Gombert, and C. Deutsch, Phys. Rev. A **23**, 924 (1981).

[29] Another prominent QSP that we used before in Ref. [11] is that of G. Kelbg, Ann. Phys. (Leipzig) **12**, 219 (1963). Though this form of QSP is known to produce results for T equilibration in weakly coupled classical plasmas that are more in line with the predictions of quantum Lenard-Balescu theory (using the Coulomb interaction) [11], we choose to use the forms of Refs. [27,28] here because (i) they have been used extensively in the past [10–13] and (ii) the sizable reduction in the equilibration rate due to their use (see Fig. 3 of Ref. [11] and Fig. 4 of this work) forces us to exhibit and address this reduction in a precise way, thereby emphasizing the distinction between quantum Coulomb plasmas and the classical QSP plasmas that we model here.

[30] The effective instantaneous temperature for each species α is commonly defined in MD as the kinetic temperature $\langle E_\alpha^{\rm kin}\rangle = \langle |v_\alpha|^2\rangle/2m_\alpha = \frac{3}{2}kT_\alpha$.

[31] H. H. Rugh, Phys. Rev. Lett. **78**, 772 (1997).

[32] F. H. Streitz, J. N. Glosli, and M. V. Patel, Phys. Rev. Lett. **96**, 225701 (2006).

[33] R. W. Hockney and J. W. Eastwood, *Computer Simulations Using Particles* (Hilger, Bristol, 1988).

[34] F. R. Graziani *et al.*, High Energy Density Phys. **8**, 105 (2012).

[35] Additionally, we have also conducted numerous simulations of classical plasmas with like charges ($e^+ - p$) and the pure Coulomb interaction, possessing the same initial conditions as those of the oppositely charged QSP hydrogen plasmas discussed here. The resulting equilibration rates follow the same trends described in detail in this work. Thus, we are confident that the conclusions we reach, delineated at the end of the Introduction, hold for plasmas with T-independent interactions as well.

[36] M. S. Murillo, Phys. Rev. Lett. **96**, 165001 (2006).

[37] A. Brunger, C. L. Brooks, and M. Karplus, Chem. Phys. Lett. **105**, 495 (1984).

[38] H. J. C. Berendsen, J. P. M. Postma, W. F. van Gunsteren, A. DiNola, and J. R. Haak, J. Chem. Phys. **81**, 3684 (1984).

[39] S. Ichimaru, *Statistical Plasma Physics, Vol. 1: Basic Principles* (Addison-Wesley, Redwood City, 1992).

[40] R. G. Dandrea, N. W. Ashcroft, and A. E. Carlsson, Phys. Rev. B **34**, 2097 (1986).

[41] A. Fetter and J. D. Walecka, *Quantum Theory of Many Particle Systems* (McGraw-Hill, San Francisco, 1971).

[42] One measure of the correctness with which these ω peaks in the integrand of Eq. (3) are included is the degree of satisfaction of the sum rule $\int_{-\infty}^{\infty} \frac{d\omega}{\omega} \mathrm{Im}[1/D(k,\omega)] = -\pi$ for each value of k.

[43] See Ref. [11] for a complete presentation of these results, together with a discussion of the differences in practical evaluations of Eq. (3) for classical QSP vs quantum Coulomb cases.

[44] The existence of a sensible 2T EOS is discussed at length by D. B. Boercker and R. M. More, Phys. Rev. A **33**, 1859 (1986). While it is far from clear that the assumptions needed to ensure the robustness of such a concept are satisfied for our MD systems (due to the possible lack of ergodicity among the slowly moving ions in particular), we adopt this framework here for practical reasons. In the end, we feel that our results justify this choice.

[45] N. W. Ashcroft and D. Stroud, Solid State Phys. **33**, 1 (1978).

[46] P. Seuferling, J. Vogel, and C. Toepffer, Phys. Rev. A **40**, 323 (1989).

[47] J. M. J. Va Leeuwen, J. Groeneveld, and J. De Boer, Physica **25**, 725 (1959).

[48] M. W. C. Dharma-wardana and M. S. Murillo, Phys. Rev. E **77**, 026401 (2008).

[49] We find that the use of so-called bridge functions, augmenting the HNC, does almost nothing to change the $g_{\alpha\beta}(r)$ and resulting V in these conditions. The bridge functions we implemented are those of H. Iyetomi, S. Ogata, and S. Ichimaru, Phys. Rev. A **46**, 1051 (1992), with the generalization to screened systems given by W. Daughton, M. S. Murillo and L. Thode, Phys. Rev. E **61**, 2129 (2000).

[50] If we adopt the ion configurational temperature of 6.777×10^4 K, rather than the nominal value of 10^5 K, in our HNC calculations of potential energy, we obtain a value of 1.44 for the right-hand side of Eq. (14), in comparison to the MD value of 1.42. This is somewhat improved over the HNC prediction of 1.33 when $T_i = 10^5$ K is used.

[51] S. Tanaka and S. Ichimaru, J. Phys. Soc. Jpn. **55**, 2278 (1986).

[52] Equation (14) for this case must be altered to reflect the fact that the electrons are quantum mechanical and are, for a density of 10^{26} cm^{-3} and a temperature of 10^7 K, borderline degenerate. However, replacing the $3N_e/2$ term in the denominator of Eq. (14) by its quantum analog [3] does not change the ratio substantively here.

[53] F. Lambert, J. Clerouin, and G. Zerah, Phys. Rev. E **73**, 016403 (2006).

[54] J. D. Kress, J. S. Cohen, D. A. Horner, F. Lambert, and L. A. Collins, Phys. Rev. E **82**, 036404 (2010).

[55] S. X. Hu, L. A. Collins, V. N. Goncharov, T. R. Boehly, R. Epstein, R. L. McCrory, and S. Skupsky, Phys. Rev. E **90**, 033111 (2014).

[56] The internal energy E predicted by our OF DFT calculations for the case $n = 10^{26}$ cm^{-3}, $T_i = 10^5$ K, and $T_e = 10^7$ K is 1304.5 eV/e^-. Our HNC-based method gives $E =$ 1386.9 eV/e^-.

[57] It is also often the case that the breakdown of Eq. (18) is not assumed and only the total free energy is given in an EOS model. In such a case, a model for the average ionization state $\bar{Z}(\rho,T)$ is constructed, from which the number of "free" electrons is inferred. Then an electronic excitation free energy $F_e(\rho,T)$ is formed from the ideal electron gas free energy for this number of electrons and the ionic free energy is defined to be the remainder: $F_i \equiv F_{\mathrm{total}} - F_e$. In this way, the assumptions of Eqs. (18) and (19) are once again imposed.

[58] We are referring to the hydrogen EOS models of, for instance, D. A. Young, High Press. Res. **16**, 389 (2000); G. I. Kerley, Sandia National Laboratories Report No. SAND2003, 2003 (unpublished); the latter of which is used by ICF designers at Lawrence Livermore National Laboratory. It should be stressed, however, that the originators of these (and other) EOS models generally did *not* intend for their models to be used in a 2T context, in the manner of Eq. (19).

[59] D. O. Gericke (private communication).

[60] This agreement is improved further if the configurational ion temperature of 6.777×10^4 K is used instead of the nominal value of 10^5 K, as in the MD-theory comparison involving Eq. (14) [50].

[61] J.-P. Hansen, I. R. McDonald, and E. L. Pollock, Phys. Rev. A **11**, 1025 (1975).

[62] A. Selchow, G. Ropke, A. Wierling, H. Reinholz, T. Pschiwul, and G. Zwicknagel, Phys. Rev. E **64**, 056410 (2001).

[63] Yu. V. Arkhipov, A. Askaruly, D. Ballester, A. E. Davletov, I. M. Tkachenko, and G. Zwicknagel, Phys. Rev. E **81**, 026402 (2010).

[64] J. P. Mithen, J. Daligault, B. J. B. Crowley, and G. Gregori, Phys. Rev. E **84**, 046401 (2011).

[65] If we use the Lindhard response function for the ions, as in Eq. (6), with $\omega \to \omega + i\gamma_i$, our results are in fact nearly identical to those employing the response function of Refs. [66,67]. Thus, the violation of local charge conservation is not particularly important here.

[66] K. L. Kliewer and R. Fuchs, Phys. Rev. **181**, 552 (1969).

[67] N. D. Mermin, Phys. Rev. B **1**, 2362 (1970).

[68] J. P. Hansen and I. R. McDonald, *Theory of Simple Liquids* (Elsevier, Amsterdam, 2006).

[69] S. A. Khrapak, Phys. Plasmas **20**, 054501 (2013).

[70] This can be further motivated by examining the Landau-Spitzer equilibration time τ, given in Eq. (8), from which we see that τ for a single species is proportional to $\sqrt{m}$ (ignoring additional mass dependences within the logarithm). Thus, $\tau_{ee} \ll \tau_{ii}$. It should be noted, however, that the Landau-Spitzer treatment, as such, is strictly only derived for thermal distributions [15].

[71] C. R. Scullard, A. P. Belt, S. C. Fennell, M. R. Janković, N. Ng, S. Serna, and F. R. Graziani, Phys. Plasmas **23**, 092119 (2016).

[72] L. G. Stanton and M. S. Murillo, Phys. Rev. E **91**, 033104 (2015).

[73] H. W. Wyld, Jr. and D. Pines, Phys. Rev. **127**, 1851 (1962).

[74] Note that the results for the analytic expression for the RPA dielectric function for arbitrary distributions, reproduced here from Ref. [71], are for the classical RPA dielectric function. Though our evaluation in the Appendix is in the context of the quantum-LB equation, we do not expect that the classical-quantum distinction in the dielectric function affects the results of Sec. IV E substantively. As explained in Ref. [71], this assumption is made strictly for mathematical convenience.